International Institute for
Applied Systems Analysis
IIASA www.iiasa.ac.at

Application of a One-Dimensional Model to Lake Balaton

Somlyody, L. and Virtanen, M.

IIASA Collaborative Paper
August 1982

APPLICATION OF A ONE-DIMENSIONAL HYDRODYNAMIC MODEL TO LAKE BALATON

L. Somlyódy
M. Virtanen

August 1982
CP-82-47

THE AUTHORS

László Somlyódy was the leader of the Balaton Case Study, Resources and Environment Area, International Institute for Applied Systems Analysis, Laxenburg, Austria. He has returned to his home institute, the Research Centre for Water Resources Development (VITUKI) in Budapest, Hungary.

Markku Virtanen is a research scholar at the Reactor Laboratory of the Technical Research Center of Finland in Otakaari, Finland.

PREFACE

One of the principal projects of the Task on Environmental Quality Control and Management in IIASA's Resources and Environment Area was a case study of eutrophication management for Lake Balaton, Hungary. The case study was a collaborative project involving a number of scientists from several Hungarian institutions and IIASA (for details see WP-80-108). One of the major tasks of the study was to find the proper description of biochemical and hydrophysical processes according to their relative importance in eutrophication. For this purpose, among others, a coupled biochemical- hydrophysical model was developed. For the hydrophysical component a three-, two-, and one-dimensional unsteady model was created. This paper reports on the simplest, the 1-D model. This is capable of characterizing the longitudinal back and forth motion in the lake. Because of its simplicity the model is well suited to study parameter sensitivity and the influence of uncertainties in the wind data. Most of the conclusions can be for multi-dimensional models.

ACKNOWLEDGMENTS

CONTENTS

APPLICATION OF A ONE-DIMENSIONAL HYDRODYNAMIC MODEL TO LAKE BALATON

L. Somlyódy and M. Virtanen

1. INTRODUCTION

A one-dimensional, transient hydrodynamic model for Lake Balaton is presented. This is the simplest acceptable approach considering the elongated shape of the lake, which accounts for the fast dynamics of the system. The research reported here is a piece of harmonized efforts, the final objective of which is to describe the spatial mass exchange properly for the eutrophication study. In other words, the relative importance of water motion and the related transport should be weighed against that of the biochemical processes.

For the present problem at least two components of water motion are of importance:

(i)   longitudinal back and forth motion (convection), a seiche type oscillation,

(ii) mechanisms causing large scale mixing, such as diffusion, horizontal circulation and vertical backflows.

Most of them have similar time and length scales as biological processes (Shanahan and Harleman 1980) consequently they cannot be neglected a priori in the framework of the water quality study and modeling. It is obvious that a 1-D approach is not capable of capturing phenomena causing mixing (item (ii)) thus a simultaneous development of a 3-D model was decided on right at the beginning. Results are reported elsewhere (Shanahan et al., 1981). An option was also maintained to work out a horizontally and/or vertically integrated 2-D model depending on the conclusions of the two other modeling exercises.

The development of the 1-D model is justifiable. First of all, it is believed that the direct coupling ofa 3-D hydrodynamic model to the biochemical component through a transport model is not the proper way to include hydrophysical effects in ecological modeling. The experiences gained for the Great Lakes (e.g., Boyce et al., 1979) support this statement. Models are becoming too large and robust, with a structure based on partial differential equations, which makes it difficult to estimate parameters for the biochemical submodel--a basic issue in ecological modeling. In another way, the gain in information does not seem to be proportional to the increase in complexity. Second, there are serious computer memory and execution time problems especially where the time horizon of water quality modeling is concerned (year or years). Third, various kinds of uncertainties exist, which question the feasibility of a detailed approach. Here, as an example, the spatial variability of the wind field is mentioned, a typical feature for mountainous regions.

Lastly, issues such as the influence of wind data uncertainty, model cali-
bration and validation, parameter sensitivity etc. can be tackled rela-
tively easily with a 1-D model and most of the conclusions extended to
more sophisticated models.

Concerning the coupling of hydrodynamic and biochemical models,
an aggregated approach is suggested, which is restricted to the descrip-
tion of temporal and longitudinal changes of water quality components.
The appropriateness of this strategy is supported by the typical longitudi-
nal gradient observed in the lake (van Straten et al., 1979) associated
with the geometrical and nutrient loading conditions (Jolánkai and
Somlyódy, 1981), by the presumably strong transversal mixing and by the
lack of a spatially refined monitoring network. This latter fact will not
allow validation of a water quality model incorporating segmentation in
the transversal direction as well.

For such a 1-D water quality model, the cross section average
streamflow Q (see (i)) can be derived from the 1-D hydrodynamic model.
It is felt that for Q this latter can be equally calibrated as in the case of
the 3-D version, which has only one additional parameter of real impor-
tance (eddy viscosity). For the calibration, dynamic water level and the
limited amount of existing velocity data can be used.

In the 1-D water quality model (a set of longitudinal dispersion equa-
tions extended by biochemical reaction terms) the influence of mixing
(item (ii)) is included in a bulk dispersion coefficient PL depending pri-
marily on wind conditions. The 3-D model can be used for calculating D_L.
The method suggested is to perform "experiments" with the model (simu-
lation of typical stormy events), and then calculate D_L from the velocity

field (e.g., as done by Fischer (1979) mainly for river problems; an alternative solution is to derive the dispersive flux directly.) Finally, the generalization of D_L as a function of wind parameters can be achieved realistically.

At present three different biochemical models are being developed (van Straten and Somlyódy, 1980) which assume that the lake can be divided into four completely mixed boxes (segments), interconnected by the hydrologic throughflow and a wind dependent exchange flow. Accordingly, the final question to be answered on the basis of the 1-D model,is whether the four boxes can be maintained and if yes, how the segments may be linked. A positive answer, among others, would be that a model structure based on ordinary differential equations could be realized, being more easily accessible to parameter estimation, identification, and sensitivity analysis.

As mentioned earlier, the development and application of the 1-D hydrodynamic model is discussed here, which is an essential element for establishing the water quality modeling procedure outlined above.

The report is organized as follows. Chapter 2 gives the background information required for model development, calibration and validation for Lake Balaton. Chapter 3 gives the governing equations and their numerical solution by an implicit finite difference method. An effective solution technique for the system of linear algebraic equations is also presented, and a careful stability analysis is performed. Subsequently, numerical tests of the algorithm carried out are presented. Chapter 4 considers model calibration and sensitivity analysis. The next chapter deals with model validation. For this purpose, several historical stormy

events are employed. In Chapter 6 a portion of the same events are simulated by including a random component in the observed wind direction. The objective of this Monte Carlo type analysis is to call attention to the input data sensitivity as compared to parameter sensitivity. Chapter 7 considers long-term computations and their evaluation. In the last chapter, conclusions are drawn.

2. BACKGROUND INFORMATION FOR MODEL DEVELOPMENT

In this chapter a summary is given on major characteristics of the lake required for the development of the present model. For more detailed information the reader is referred to Muszkalay (1973), Györke (1975), Béll and Takács (1974), Somlyódy (1979), and Shanahan et al., (1981).

The lake is long and narrow (78 km by roughly 8 km, see Fig. 1) and extremely shallow. The average depth is 3.14 m and is everywhere less than 5 m deep, except in one small area at the Tihany peninsula which divides the lake. A sudden contraction occurs formed here and the cross-section area changes in 3-4 kms distance by a factor of 6-7. In this region, a river type water motion is observed, which changes direction depending on wind conditions and the associated water level oscillation. The velocity may exceed 1 m/s, a very high value (Muszkalay, 1973) while in other areas of the lake it is generally less than 0.1 - 0.15 m/s. The shallowness of the lake permits a water motion response even to mild winds and also because of the fluctuations in the wind field, a steady state never exists. This is well demonstrated by the velocity measurements of Shanahan et al. (1981).

The prevailing wind direction lies between NW and N. This is even more pronounced if events of strong winds (> 8m/s) and summer periods are considered (Béll and Takács, 1974). The second most frequently occurring directions are SE, ESE, and SW which may dominate in autumn and winter time. The monthly average velocity ranges from 2 to 5 m/s, however, the maximum value may reach 30 m/s (Fig. 2). The hourly average wind exceeds the 8 m/s value at Siófok approximately during 15% of a year (Béll and Takács, 1974). The number of seiche type events (specifically, seiche is the lake's response to a single wind impulse) reaches 1000 in a year (Muszkalay, 1979).

The temporal and spatial changes in wind are strongly influenced by the surrounding hills of the northern shoreline. Hills cause not only a nonuniform wind distribution along the northern shoreline, but also a highly variable velocity field above the lake, due to sheltering, channeling, deviating, and separating effects of mountains and valleys (the position of the latter is generally perpendicular to the lake's axis). The average wind characteristics clearly point to this phenomenon. For instance, at the eastern end of the lake the prevailing direction is NW, at the other end N, while in the middle on the southern shoreline NE (Béll and Takács, 1974). The spatial changes in the direction are clearly indicated by a comparison of the records for Keszthely and Siófok for 1977 (8 observations per day). Accordingly for W > 3 m/s, the mean value of the difference in angle is 39 degrees, while its standard deviation is 36 degrees, resulting in a very wide domain in which the direction can range in space above the lake. Due to the sheltering effect mentioned above, the average wind speed is higher by 40-60% at Siófok than at Keszthely. This effect recurs

consistently, as is clearly indicated by Fig. 3, which shows the daily average wind speed in 1977 for three stations (see also Fig. 1). The longitudinal component, which is of importance for the 1-D approach, is given in Fig. 4.* The regions richest in wind energy are the Szigliget Bay (Fig. 1) and the eastern end of the lake. From the presence of mountains and the "smoothness" of water surface contrasted to the "roughness" of the surrounding topography also a transversal non-homogeneity follows. Observations made on ships plying between Siófok and Füred (Fig. 1) clearly indicated for NW wind conditions a continuous reduction in speed, up to 40%, after leaving a roughly 3 km wide southern zone.

The number of wind recording stations (Siófok, Szemes, Keszthely, and some provisional gauges, see Somlyódy 1979) does not allow accurate specification of the wind field characterized above. Thus, in the present modeling effort, the uncertainty associated is stressed and will be accounted for.

The most detailed study on the lake's water motion was performed by Muszkalay (1973) who collected a decade of water surface elevation observations at up to ten stations around the lake (Fig. 1). Simultaneous measurements of wind speed at one or two stations and occasionally of water current in the strait of Tihany complete his data base. The measurement shows the lake to be in seemingly constant motion, as already stressed. A strong wind of only a few hours duration can lead to considerable oscillations. A typical month-long record showing both longitudinal

---

It is stressed that the continuous record or the hourly values being generally used for modeling purposes would give a much more scattered picture compared to Fig. 3 (for example the standard deviation of W^2 within a day derived from hourly values has the same magnitude than the daily average, $\overline{W}^2$, see Somlyódy, 1980).

and transversal modes is given in Fig. 5. The data are well suited to study seiche, combined oscillations, denivellation etc. (see Muszkalay, 1973) and serve as a basis for model development.

Having his observations Muszkalay selected typical stormy events and looked for empirical relationships for the maximal longitudinal denivellation along the lake and velocity at the strait as a function of wind parameters. Based on a regression analysis the following equations were gained (Muszkalay 1973)

$$I = 0.38 \times 10^{-6} \, T^{0.25} \, (W_x - 2.8) \quad \text{if} \quad |\alpha^*| < 22.5° \qquad (1a)$$

$$I = 0.105 \times 10^{-6} \, T^{0.25} \, (W_x + 13.5)^{-0.16} \quad \text{if} \quad |\alpha^*| > 22.5° \; , \qquad (1b)$$

and

$$U^* = 500 \, I^{0.5} - 0.5 \; . \qquad (2)$$

Here W_x is the longitudinal component of maximum instantaneous wind speed observed during the storm (measured at Szemes, Fig.(1)), $\alpha^* = \alpha - 247.5$ the angle between the velocity vector and the lake's axis ($|\alpha^*| \leq 90°$) and T the duration of the storm [h] (T $\leq$ 12h). In Eqs. (1a) and (1b) the maximum longitudinal denivellation [-] is determined from the difference of extreme stages at Keszthely and Kenese. It is a fictitious quantity in the sense that these extremes may not, in fact, occur at the same time (the lag is however not large). U^* is the maximum velocity during the event in standard cross-section Nr. 25 (VITUKI 1976) at a vertical measured 250 m from the northern shore, 1 m below the free surface. The cross-section area is here approximately 4000m^2 and $U = (0.8 - 1.0) \, U^*$, (Muszkalay, 1981, personal communication), U cross-section average value.

- 9 -

Since Eqs. (1) - (2) will be effectively used later further comments are given here on their features:

(i)   as is apparent from Fig. 2, the specification of T also depends on subjective judgement;

(ii) the instantaneous peak wind speed, W_{max}, is essentially larger than the peak for a reasonable averaging period, (e.g., an hour, see again Fig. 2), $\bar{W}_{max}$. Based on a statistical analysis on historical data the ratio moves around 1.2 - 1.3;

(iii) I linearly depends on W_{max} although theory suggests a quadratic relationship. It is noted however that most of the data utilized lay in the 5 - 12 m/s wind speed domain if $|\alpha^*| < 22.5$ (see Muszkalay, 1973) and a quadratic fitting could have been also done;

(iv) for $|\alpha^*| > 22.5, I > 0$ if $W_x = 0$, a clear indication of the non-homogeneity in the wind field;

(v)   there was not enough data available to find a continuous function between I and α^*;

(vi) within 12 h I did not reach complete saturation.

On the whole,however, Eqs. (1) - (2) comprise the major features of the system and as such are well applicable for model calibration. Major advantages are that simplified stormy events (parametrized, e.g., by one velocity, direction and duration values, respectively) can be satisfactorily employed and time can be eliminated in the course of the evaluation (see later). Because of issues (i) - (vi) a perfect agreement to Eqs. (1) - (2) is certainly not expected. It is stressed that following the calibration, real historical scenarios should be used for validation.

3. MODEL DEVELOPMENT

3.1. Governing Equations

Water motion along the lake's axis x (see Fig. 1) is described by the one-dimensional equations of motion and continuity often adapted for river flow situations (Mahmood and Yevjevich, 1975; Kozák, 1977):

$$\frac{\partial U}{\partial t} = -g\frac{\partial z}{\partial x} - \frac{1}{2}\frac{\partial}{\partial x}(U^2) + \frac{1}{H\rho}(\tau_s + \tau_b) \ , \tag{3}$$

$$\frac{\partial A}{\partial t} = -\frac{\partial Q}{\partial x} \ , \tag{4}$$

where the latter can be written as

$$B\frac{\partial z}{\partial t} = \frac{\partial}{\partial x}[UB(H_1 + z)] \ . \tag{4a}$$

Here $U = Q/A$ longitudinal flow velocity averaged over cross-section, $A = B(H_1 + z)$, Q streamflow rate, z water level elevation, B width, H_1 non-disturbed water depth, $H = H_1 + z$ real depth, τ_s wind shear stress at the water surface, τ_b friction shear stress at the bottom, ρ water density and g gravity acceleration.

Using the definition of U and A, furthermore Eq. (4), Eq. (3) can be rearranged and the following set of equations should be solved:

$$\frac{1}{A}\frac{\partial Q}{\partial t} = -g\frac{\partial z}{\partial x} - 2\frac{Q}{A^2}\frac{\partial Q}{\partial x} + \frac{Q^2}{A^3}\frac{\partial A}{\partial x} + \frac{1}{H\rho}(\tau_s + \tau_b) \ , \tag{5}$$

$$B\frac{\partial z}{\partial t} = -\frac{\partial Q}{\partial x} \ , \tag{6}$$

$$A = A_1 + Bz \ , \tag{7}$$

$$H = H_1 + z \ , \tag{8}$$

where A_1 belongs to the motionless water level and it is assumed that $B(z) = $ const. for small $|z|$.

The shear stresses are described by introducing the drag coefficient C_D and bottom friction coefficient λ (see e.g., Lick, 1976; Virtanen, 1978):

$$\tau_s = \rho_a \, C_D \, W_x \, |W| \qquad (9)$$

$$\tau_b = -\rho \, \lambda \, U \, |U|^n = -\rho \, \lambda \, \frac{Q \, |Q|^n}{A^{1+n}} \qquad (10)$$

where ρ_a is the air density, W and W_x wind speed and its longitudinal component, respectively, and n the bottom friction exponent $(o \leq n \leq 1$; here the quadratic law will be used, $n = 1$).

On account of mathematical and physical reasoning, dimensionless quantities will be introduced (e.g., elements of the same magnitude can be arrived at in matrices to be inverted, an essential numerical advantage). As scaling factors, typical depth, width, length and velocity $H_0, B_0, L_0,$ and U_0, respectively, will be employed as follows:

$$Q^* = \frac{Q}{H_0 B_0 U_0} \ ,$$

$$z^* = \frac{z}{H_0} \ ,$$

$$A^* = \frac{A}{H_0 B_0} \ ,$$

$$B^* = \frac{B}{B_0} \ , \qquad (11)$$

$$H^* = \frac{H}{H_0} \ ,$$

$$x^* = \frac{x}{L_0} \ ,$$

$$t^* = \frac{t \, U_0}{L_0} \ ,$$

$$W^* = \frac{W}{U_0} \ ,$$

and

$$W_x^* = \frac{W_x}{U_0} \ .$$

Applying these expressions and dropping the asterisk notation, Eqs. (5)-(7) will be transformed to

$$\delta_4 \frac{Fr}{A} \frac{\partial Q}{\partial t} = - \frac{1}{Fr} \frac{\partial z}{\partial x} - (\delta_2 + \delta_3) Fr \frac{Q}{A^2} \frac{\partial Q}{\partial x} +$$

$$+ \delta_3 Fr \frac{Q^2}{A^3} \frac{\partial A}{\partial x} + r_w Fr \frac{1}{H} W_x |W| - r_b Fr \frac{1}{H} \frac{Q |Q|^n}{A^{1+n}} , \qquad (5a)$$

$$B \frac{\partial z}{\partial t} = - \frac{\partial Q}{\partial x} \qquad (6a)$$

$$A = \frac{A_1}{H_0 B_0} + \delta_1 Bz \qquad (7a)$$

$$H = \frac{H_1}{H_0} + \delta_1 z , \qquad (8a)$$

where Fr is the Fronde number

$$Fr = \frac{U_0}{\sqrt{gH_0}} , \qquad (12)$$

r_w and r_b wind and bottom friction parameters, respectively

$$r_w = \frac{\rho_a}{\rho} C_D \frac{L_0}{H_0} \qquad (13)$$

$$r = \lambda \frac{L_0 U_0^{n-1}}{H_0} \qquad (14)$$

In the system of equations three nonlinear effects are incorporated such as

(i) the effect of water elevation on A and H,

(ii) the role of the time derivative of Q/A through the continuity, and

(iii) the convective acceleration.

Simultaneously with the scaling, each of the corresponding terms and in addition, also the term $\frac{\partial Q}{\partial t}$ were supplied by an artificial coefficient δ_i ($\delta_i = 0$ or 1, i = 1...4), in order to make possible a separate study on their relative importance (note if $\delta_i = 0$, i = 1...4, the diffusive wave equa-

tion, while if in addition $\partial z / \partial x = 0$ it results in the kinematic wave equation). It has to be mentioned that the bottom friction obviously also causes nonlinearity if $n \neq 0$.

3.2. Initial and Boundary Conditions

As initial conditions, $Q(0,x)$ and $z(0,x)$ should be given. Most frequently a nondisturbed initial state is assumed, leading to $Q(0,x) = z(0,x) = 0$.

Boundary conditions for one of the variables should be specified at the two ends of the lake $x = 0$ and $x = L$, respectively. For lake problems generally $Q(t,0)$ and $Q(t,L)$ are given. If no inflow and outflow take place, as will be assumed here, $Q(t,0) = Q(t,L) = 0$.

3.3. Numerical Solution

Bearing in mind criterion of consistency, stability, convergency, and accuracy of the numerical solution, furthermore the need for a fast method on computer for allowing the simulation of a year or a couple of years an implicit finite difference scheme (Mahmood and Yevjevich, 1975) is selected to which a matrix sweep technique is coupled.

3.3.1. Finite difference scheme

Time derivatives are approximated by differences centered in space and time

$$\frac{\partial f}{\partial t} = \frac{1}{2\Delta t} [(f_i + f_{i+1})^{j+1} - (f_i + f_{i+1})^j] \ , \tag{15}$$

while for space derivatives the differences are centered in space but weighted in time

$$\frac{\partial f}{\partial x} = \frac{1}{\Delta x_i}[\ \vartheta\ (f_{i+1} - f_i)^{j+1} + (1 - \vartheta)\ (f_{j+1} - f_i)^j\ ]\ . \tag{16}$$

Superscripts j and i refer to time and location in space, respectively, Δt and Δx_i are the corresponding increments (Δx is not necessarily equidistant) and ϑ weighting parameter, $\vartheta = 0.5 - 1$ (see e.g., Liggett and Cunge, 1975). The scheme is unconditionally stable in the given range for ϑ. Accuracy reasons suggest a value near to 0.5. For the coefficients and non-derivative terms in Eqs. (5a) - (8a) space-centered, forward-time approximations are employed

$$[f]_i^j = \frac{1}{2}(f_i + f_{i+1})^j\ . \tag{17}$$

For bottom shear, however, a more detailed approach, centered in space but weighted in time is used ($0.5 \le \vartheta_1 \le 1$).

$$S = -r_b\ \frac{1}{H}\ \frac{Q\ |Q|^n}{A^{1+n}} = \frac{\vartheta_1}{2}(S_i + S_{i+1})^{j+1} + \frac{1 - \vartheta_1}{2}(S_i + S_{i+1})^j\ , \tag{18}$$

and S^{j+1} is calculated through linearization

$$S_i^{j+1} = S_i^j + \left[\frac{\partial S}{\partial t}\right]_i^j \Delta t =$$

$$= S_i^j + \left[\frac{\partial S}{\partial z}\frac{\partial z}{\partial t} + \frac{\partial S}{\partial Q}\frac{\partial Q}{\partial t}\right]_i^j \Delta t$$

$$= S_i^j + \left[-\frac{2+n}{H}\ S\ \frac{\partial z}{\partial t} + \frac{1+n}{Q}\ S\ \frac{\partial Q}{\partial t}\right]_i^j \Delta t\ . \tag{19}$$

The space and time centered scheme (15) is then used for time derivatives in Eq. (19).

With these approximations and by defining new variables

$$u_i = Q_i^{j+1} - Q_i^j \tag{20}$$

$$v_i = z_i^{j+1} - z_i^j\ ,$$

from the equations of continuity and motion the following system of linear algebraic equations results.

$$A_{1i}u_i + A_{2i}v_i + A_{3i}u_{i+1} + A_{4i}v_{i+1} = A_{5i} \quad . \tag{21}$$

$$B_{1i}u_i + B_{2i}v_i + B_{3i}u_{i+1} + B_{4i}v_{i+1} = B_{5i} \quad . \tag{21}$$

The coefficients $A_{1i} \cdots A_{5i}$, $B_{1i} \cdots B_{5i}$ are given in Appendix I.

3.3.2. Solution of the system of linear algebraic equations

Since i ranges from 1 to (N-1), Eq. (21) leads to (2N-2) equations closed then by the boundary conditions for 2N unknown variables. In practical cases the number of equations to be solved at each time level may exceed some hundred or thousand resulting in an unrealistic execution time when using traditional solution techniques. For this reason a matrix sweep method is developed here which is a modified version of the computationally efficient double sweep technique originally established by Preissmann (see e.g., in Mahmood and Yevjevich, 1975). The essence of the method is based on two features of the present problem:

(i)   Eq. (21) is linear.

(ii) A boundary value problem is handled (u_1 and u_N are known). These properties allow computation of the new values at level (j + 1) from i to (i + 1) in an explicit fashion rather than deriving all the unknown variables simultaneously in one step.

For purposes of clarity Eq. (21) is rearranged to a matrix form

$$\underline{A}_i \underline{y}_{i+1} = \underline{B}_i \underline{y}_i + \underline{c}_i \tag{22}$$

where

$$\underline{y}_i = \begin{bmatrix} v_i \\ u_i \end{bmatrix} \quad , \quad \underline{y}_{i+1} = \begin{bmatrix} v_{i+1} \\ u_{i+1} \end{bmatrix} \quad ,$$

and the $\underline{A}_i$ and $\underline{B}_i$ matrices and the $\underline{c}_i$ vector include the known coefficients $A_{1i} \cdots A_{5i}$, $B_{1i} \cdots B_{5i}$. Since the linear relation between $\underline{y}_{i+1}$ and

y_i stated by Eq. (22) is satisfied for all i values, $1 \leq i \leq (N-1)$, it also exists between y_N and y_1. Accordingly, one may select in two subsequent steps arbitrary values $v_1^{(1)}$ and $v_1^{(2)}$ and compute the corresponding output vectors $y_N^{(1)}$ and $y_N^{(2)}$. The accurate y_N value fulfilling the boundary conditions can then be gained from the linear combination of $y_N^{(1)}$ and $y_N^{(2)}$.

As all the matrices and vectors A_i, B_i, and c_i are known in advance a direct relationship can be achieved between y_N and y_1 by the repeated use of Eq. (22) as follows

$$y_2 = A_1^{-1} \, B_1 \, y_1 + A_1^{-1} \, c_1 \tag{23}$$

.

.

.

.

.

.

$$y_N = \left[\prod_{i=N}^{1} A_i^{-1} \, B_i \right] y_1 + \sum_{i=1}^{n} \left[\left(\prod_{j=N}^{i+1} A_j \, B_j \right) A_i^{-1} \, c_i \right] \, ,$$

or

$$\begin{bmatrix} v_N \\ u_N \end{bmatrix} = \begin{bmatrix} a_{11} & a_{12} \\ a_{21} & a_{22} \end{bmatrix} \begin{bmatrix} v_1 \\ u_1 \end{bmatrix} + \begin{bmatrix} b_1 \\ b_2 \end{bmatrix} \, , \tag{24}$$

from which provided that $a_{21} \neq 0$

$$v_1 = \frac{1}{a_{21}} \, (u_N - a_{22} \, u_1 - b_2) \tag{25}$$

follows. The computation of y_i can then be recursively performed using Eq. (22) or (23). Comparison of the value u_N derived with the boundary

- 17 -

condition specified gives a direct idea of the magnitude of round-off errors (see later).

After getting u_i, v_i, the new values of streamflow rate, water level, depth, and cross section area are calculated as follows:

$$Q_i^{j+1} = Q_i^j + u_i$$
$$z_i^{j+1} = z_i^j + v_i$$
$$H_i^{j+1} = H_i^j + \delta_1 v_i$$
$$A_i^{j+1} = A_i^j + \delta_1 B_i v_i \ .$$

(26)

The same procedure is repeated on the subsequent time levels.

The essential feature of the method developed is that due to the decomposition outlined N number 2 x 2 matrices should be inverted as contrasted to the inversion of a single matrix of 2N x 2N dimension. Thus the number of elementary operations and execution time is proportionate to N rather than to N^3. A different advantage associated with the matrix treatment is that stability can be relatively easily analysed, the subject of the subsequent section.

3.3.3. Stability

As was noted before, the implicit finite difference algorithm adopted is unconditionally stable in time for the "background weighted" parameter values $\vartheta \geq 0.5$ (Mahmood and Yevjevich, 1975). In the present solution technique, however, within each time level as well the new values are generated recursively from the boundary to the interior. Thus the error propagation in space must be separately analyzed.

Thanks to the small size of the amplification matrix $A_i^{-1} B_i$, its eigenvalues λ_1, λ_2 and eigenvectors can be even analytically solved. With them

the amplification matrix can be transformed to diagonal form

$$\Lambda_i = \begin{bmatrix} \lambda_1 & 0 \\ 0 & \lambda_2 \end{bmatrix} = \underline{P}_i^{-1} \, \underline{A}_i^{-1} \, \underline{B}_i \, \underline{P}_i \tag{27}$$

provided that the transformation is well defined ($||\underline{P}_i^{-1}|| \; ||\underline{P}_i|| < K < \infty$). Then its stabilizing properties can be described and analyzed by means of eigen values (see Appendix II).

Since the system of equations is unconditionally stable in time, the "strong stability" $||\underline{A}_i^{-1} \, \underline{B}_i|| < 1$ is not absolutely necessary in space. The value of the acceptable upper limit $||\underline{A}^{-1} \, \underline{B}||_0$ for $||\underline{A}_i^{-1} \, \underline{B}_i||$ depends on the number of grid points N and on the desired accuracy ε. An initial error $\underline{\varepsilon}_i$ ($|\underline{\varepsilon}_i| < \varepsilon_0$) at $i = 1, \ldots, N - 1$ will be amplified to the end of the basin to

$$\underline{\varepsilon}_N = \prod_{j=N}^{i+1} (\underline{A}_j^{-1} \, \underline{B}_j) \; \underline{A}_i^{-1} \, \underline{\varepsilon}_i \tag{28}$$

satisfying $||\underline{\varepsilon}_N|| < \varepsilon$ if $||\underline{A}^{-1} \, \underline{B}||_0 < (\varepsilon / \varepsilon_0)^{\frac{1}{N-1}}$.

A practical measure for $\underline{\varepsilon}_N$ is the difference between the given boundary value Q_N^i and the value $Q_N^{i-1} + u_N$ computed through the algorithm. Since no direct evidence of the actual origin of the initial error is available only a qualitative (or statistical) confirmation of these relations is possible by numerical tests (see later).

The analysis of the matrix norm takes a somewhat different form according to whether certain elements are zero or not. Besides, on non-linear terms this depends on two factors, viz. on the explicit inclusion of the time-derivative to the equation of motion ($\delta_4 = 0$ or 1) and on the bottom friction and velocity ($\vartheta_1 r_b \, |U_i|^n$ and U_i), (see Appendix II).

Figure 6 illustrates the behavior of the matrix norm as a function of the time-step in the four different situations deriving from two independent binary value parameters (δ_4 and $r_b\,\vartheta_1\,|U_i|^n = 0$ or $\neq 0$):

1° As can be seen for the frictionless diffusion wave approach ($\delta_4 = 0$) stability is improved by enlarging the time-step (Fig. 6a).

2° Still for a frictionless case, but with local acceleration ($\delta_4 = 1$) a singularity exists (Fig. 6b) which defines a critical time step Δt_{cr} (infinite error amplification in space)

$$\frac{2\,\vartheta\,\Delta t_{cr}}{\Delta x_i}\,\frac{\sqrt{H_i}}{Fr} = 1 \ . \tag{29}$$

Either sufficiently small or large time-steps lead to stability.

3°, 4° Inclusion of nonzero friction makes stability depend on local velocity U_i which varies within large limits and will result in formally a

$$\frac{2\,\vartheta\,\Delta t_{cr}}{\Delta x_i}\,\frac{\sqrt{H_i}}{Fr} = f\,(r_b,\,\vartheta_1,\,n,\,U_i) \tag{30}$$

type relationship (for details see Appendix II). With positive velocities the singularity observed in Figure 6b is shifted towards larger time-steps simultaneously increasing the matrix norm at large values of $\dfrac{2\,\vartheta\,\Delta t}{\Delta x_i}\,\dfrac{\sqrt{H_i}}{Fr}$. The amplifying matrix norm should be sufficiently limited with all possible velocity values and for this reason quite a wide range of time-steps must be ruled out. In principle, the corresponding graphs (Figs. 6c and d) are similar to that of case 2°, but due to the character of Figure 6c only large time increments are acceptable.

For practical applications it is advisable to select Δt to be as large as possible. An upper limit is given by the period of free oscillations T, in the

lake and by the accuracy desired. For coarse description values of T/10...T/2 and even more might be suitable (see later). Stability can be improved by increasing the interpolation parameter ϑ, but this will cause numerical damping (see later), so $\vartheta = 0.5$ is preferable. Bottom friction weighting parameter ϑ_1 is relatively ineffective on stability.

Since the bottom friction coefficient, r_b should be established through calibration, Δx_i is the other essential parameter to control stability. On the basis of lake geometry it can be selected quite freely. As a guideline Figure 6 and Eqs. (29) and (30) can be used to harmonize Δt and Δx_i.

3.4. Numerical Tests of the Algorithm

Numerical properties of the solution algorithm and the correctness of its computer realization were checked by a number of test simulations for rectangular basins and simple conditions. Two basic examples were considered for which analytical solutions can be derived:

(i)   Initially a motionless, sinusoidal water level with amplitude E is given which then begins to oscillate under the influence of gravity. No winds, boundary currents and friction are assumed, furthermore nonlinear terms are neglected.

(ii) A still and level water body is assumed, on which a uniform constant wind acts (step-like wind input). The water level converges through oscillations to the steady state (set-up) where the water surface lies inclined against the wind and no currents exist. Next only example (i) is discussed. About test case (ii) it is briefly noted that the assymptotic behavior of the system was satisfactorily reproduced

(see also Fig. 13 in the subsequent chapter).

A basin similar in geometry to Lake Balaton (length 80 km, width 8 km, depth 3.3 m, theoretical seiche period $T = 2L/\sqrt{gH} = 7.5h$) was selected and with scaling $Fr = 1$ realized (as space step $\Delta x = 2000m$ was used). For the frictionless situation without nonlinear terms the critical time step (see Eq. 29) is given by $\vartheta \, \Delta t_{cr} = 174s$.

For $\vartheta < 0.5$ the solution was stable and accurate provided that $\Delta t < \Delta t_{cr}$. For $\vartheta = 0.5$ satisfactory solutions were produced both for small and large time steps ($\Delta t \neq \Delta t_{cr}$). $\Delta t = T/4$ resulted in still satisfactory agreement both for amplitude and phase, but besides $T/4$ a small numerical lag in the wave propagation started to appear. Finally, with very large time steps $\Delta t > T$ also the wave amplitude was damped. For $\vartheta > 0.5$ similar behavior was observed but with a strong numerical damping (even if ϑ were close to 0.5, between 0.575 and 0.65). Based on the simulation results the computed boundary error ε_N was analyzed. This followed roughly the relation

$$\varepsilon_N \cong \left[2 \; \frac{1 + 6x + x^2}{(1 - x)^2} \right]^{\frac{N}{2}} \varepsilon_0 \quad , \tag{31}$$

with $x = 2\sqrt{gH} \; \vartheta \, \Delta t / \Delta x$ and $\varepsilon_0 = 10^{-25}$. With friction, a much more casual behavior of the boundary error appeared. With Δt in the critical region $\Delta t_{crmin} \leq \Delta t \leq \Delta t_{crmax}$ (see Figs. 6c and d) an instability was seldom met. Outside this region no instability was observed.

The test examples justified the applicability of the algorithm developed. The experiences gained in practice also proved that "weak stability" is sufficient. Based on the analysis outlined $\Delta t < 100s$ or $\Delta t > 1000s$

can be adapted for the present problem if $\Delta x = 2000$m (in the majority of cases 1800 or 3600 s will be used for Δt). For reasons of accuracy, $\vartheta = \vartheta_1 = 0.5$ is suggested. The computations performed also support the adequacy of stability analysis which was mainly of a linear nature and, in as much as based on the concept of eigen values, strictly justified for the case of constant coefficients; a condition which will not be satisfied in practice.

Finally, it is mentioned that the influence of nonlinear terms discussed in Section 3.1 is negligible in most of the cases. The same is not valid for the term $\partial Q / \partial t$ thus the diffusive wave approach cannot be applied. It is also noted that the matrix sweep technique turned out to be faster roughly by two orders of magnitude on the computer than conventional inversion techniques for the original system of equations (21).

4. SENSITIVITY ANALYSIS AND MODEL CALIBRATION

As mentioned earlier, in the course of the calculations for Lake Balaton, $\Delta x_i = \Delta x = 2000$ m was chosen. The parameters of 40 cross-sections (A_i, B_i and H_i) were established on the basis of geometrical data of standard cross-sections (VITUKI, 1976). For runs presented here the time step Δt was 1800 s ($\Theta = \Theta_1 = 0.5$ and n = 1). The wind input, of rectangular profile most used in this chapter was numerically represented by $m = T / \Delta t + 1$ number of nonzero wind velocity values, $W_j = W = $ const ($1 \leq j \leq m$, T the duration of the event).

- 23 -

4.1. Sensitivity Analysis

Subsequently, the influence of geometric data, bottom friction coefficient, drag coefficient, the appropriateness of rectangular wind profile, and the description of the wind field are discussed. As a point of reference, the parameter values of the final calibration (see Section 4.2) is used (C_D = 0.0013 and λ = 0.003 for the two most important parameters).

4.1.1. Geometry

A numerical representation of the lake for the 1-D treatment fulfilling some global criteria (total volume and surface area, etc.) can be relatively easily realised. The major problem is given by the approximation of the lake's geometry in the vicinity of the peninsula forming a Venturi type structure (see Fig. 7 for the cross-section area) which results in nearly half of the energy loss from friction in the system. In this region it is of major importance that the discretization adapted (note that many possible methods exist) should be well harmonized with the numerical formulation of the problem and give the same friction loss (the locally dominating term in Eq. (3)) as a continuous description. The relevance of this argument is well illustrated by Fig. 8 which shows how extremely sensitive the solution is (maximal denivellation and the discharge at the peninsula) on the single cross-section area at Tihany (Nr. 25, see Fig. 7, or i = 28 in the model).

Keeping in mind Eq. (10) and assuming that Q(x) $\approx$ const. in the vicinity of the peninsula (defined by coordinates x_1 and x_2), a satisfactory approximation of the friction term is achieved if

$$k = \int_{x_1}^{x_2} \frac{dx}{A^2(x)} \tag{32}$$

is approached properly with the use of Eq. (17). Given k on the basis of Fig. 7, a single equation is obtained for A_{27}, A_{28}, and A_{29} and any feasible combinations of these can be adapted (this is well proved by model simulations--a more accurate procedure). The selected values are given in Fig. 7. It is apparent that the throat cross-section is slightly higher than the real one, simply no realistic combination with smaller A_{28} exists. Because of this minor difference, the use of discharge is preferred for calibration in Section 4.2 over velocity.

4.1.2. Bottom friction coefficient

This is the most essential model parameter which influences not only the maximal denivellation and discharge but also the damping. This is well illustrated by Fig. 9 showing the water level oscillation at one end of the lake, Keszthely. The wind input was characterized by T = 2 h and W_x = 8 m/s. The friction coefficient, λ, ranged in a wide, but still realistic domain, 0.0075 - 0.024. For small λ the first and second amplitudes are nearly equal, while for large value the oscillation is practically completely damped out after the first half period. The pattern is similar for Q(t) with a slightly smaller damping effect.

The influence of λ can be more easily captured and the sensitivity analysis better used for the purpose of calibration if the maximal denivellation defined by the second and first amplitudes, respectively, $I^{(2)}$ / $I^{(1)}$, are considered. As can be seen from Fig. 10, the water level is relatively insensitive on λ in the vicinity of the nominal value λ_0 = 0.003 (see later). In the domain (0.25, 8) for λ/λ_0, I moves in the +15, -25% range. The velocity at Tihany shows a higher sensitivity, while the most pronounced

changes can be observed on $I^{(2)}/I^{(1)}$. It is noted that a similar figure was gained also for wind events of longer duration.

4.1.3. Wind drag coefficient

Because of the uncertainties in the wind field, no attempt was made to consider C_D as a function of wind speed or other parameters (see, e.g., Wu 1969; Graf and Prost 1980; Shanahan et al. 1981). As indicators for the sensitivity the same parameters, I/I_0 and Q/Q_0 were employed. Fig. 11 shows the expected linear dependence for water level from which a quadratic relationship follows for the longitudinal component of the wind speed. The change in Q has a slightly non-linear tendency.

Obviously, C_D's being directly related to the wind energy input to the water body, has a major influence on both I and Q. λ associated with the bottom shear has an opposite effect. From the complementary character of Figs. 10 and 11 follows that there is no unique, "best" parameter vector, but several combinations of λ and C_D can give approximately the same results for I and Q. The knowledge of the damping properties of the system is consequently very important (see β_3 in Fig. 10): information which helps to fix the reasonable range for λ and subsequently also for C_D (see later).

4.1.4. Wind profile

The rectangular wind input will be used later for calibration as well. In reality, however, no such event occurs. In addition, many different profiles can be specified by the same parameters, T and W_x (see Chapter 2). Although the appropriateness of the model and parameter values

found in calibration should be justified through validation, still it is obviously advisable to test the model sensitivity on the input profile in advance.

Here the results for one type of distribution is presented. The profile was specified by radial lines as shown in Fig. 12. The wind set up occurs gradually, depending on n_1, the number of time steps when $W^j \neq 0 \neq W_{max}$ ($n_1 = 0, 1, ..., 4$).

Two situations were realized:

$1°$ $W_{max} = 8m/s$

$2°$ $\overline{W} = 8m/s$, $W_{max} \geq 8m/s$, where the overbar indicates averaging for period T.

The results for β_1 and β_2 are given in Fig. 12. As can be seen the sensitivity is slightly higher for the case $2°$. If however results of type $2°$ were related to that gained with the corresponding W_{max} values (8, 8.47, 9, 9.6, and 10.3 m/s for n = 0...4), but of a rectangular distribution, practically $1°$ curves were obtained again. This suggests that W_{max} is appropriate for characterization of a storm,as used by Muszkalay (see Section 2) and furthermore that the results are not necessarily sensitive to the shape of the wind input. In fact, if the length of the set up is restricted to 1.5 h (n = 3), a relatively long period compared to the duration of the storm, an error still smaller than 10% is resulted in. Consequently the rectangular profile can be satisfactorily used for model calibration.

It is noted, that another profile family similar in concept to the previous one, but symmetrical to T/2, was also tested. Similar experiences were gained with somewhat higher sensitivity. This example was found

less typical since the maximal I and Q values do not depend on wind abatement and the symmetric character causes a higher distortion in $W_{max}/\bar{W}$.

4.1.5. Description of the wind field

From the characterization of the wind field in Section 2 both deterministic and stochastic changes in wind parameters (absolute value, $|W|$ and angle α) follow. Here the first type of variation is dealt with. Three phenomena are accounted for:

(i) linear wind speed distribution along the lake

$$|W| = [(1 - a_0) + (1 + a_0)\frac{x}{L}] |W_{L/2}| \qquad (33)$$

where $W_{L/2}$ can be approximated by observations done at Szemes (or by the arithmetical mean of speeds measured at Keszthely and Siófok, respectively). Based on a statistical analysis of data for 1977 (see Fig. 3) and the explanation given in Section 2, a_0 ranges between 0.1 - 0.2. Here also utilizing the results of several test simulations $a_0 = 0.15$ will be employed. a_0 modifies primarily the ratio of water level amplitudes measured at the two ends of the lake, and has a slight influence on I and Q.

(ii) longitudinal distribution of α

The information available (see Section 2) clearly indicates that α is not uniform along the lake. The findings of Muszkalay suggest that even if the wind direction is perpendicular to the lake's axis at one measurement station, the same condition is not true for the largest portion of the water surface. Consequently, zero longitudinal deniv-

ellation can rarely be observed unless W is very small.

Here various hypotheses were made on $\alpha(x)$ and tested whether they may lead to a better description of the back and forth motion, especially if $|\alpha - 274.5|$ is small, or not. Since the final conclusion was negative, $\alpha(x) = $ const. is assumed subsequently. An example will be given later in relation to the issue in question.

(iii) change of the wind direction across the lake

The wind direction changes also across the water surface and its average value above the water surface differs from the observed α at the southern shoreline (Szemes). This effect is important if the disturbing influence of hills (see Section 2) becomes dominant.

Based on simple aerodynamic considerations it was assumed that the series of hills act as a cascade, causing an increasing deviation in the wind direction, followed by a separation zone, as α moves from 247.5° (the angle of the lake axis) to 337.5°. This hypothesis was introduced by the modification of the longitudinal wind force (see Eq. (57)) if $0 < \alpha^* = \alpha - 247.5 \leq 180$

$$W_x \, |W| = W^2[f(\alpha^*)\cos\alpha^* + k_1 \sin^n \alpha^*] \, , \qquad (34)$$

where

$$f(\alpha^*) = \frac{1}{4}\{1 + \cos[(1 + \sin\alpha^*)\alpha^*]\}^2 \, , \qquad (35)$$

and the parameter values were fixed to $k_1 = 0.1$ and $n = 0$. If $\alpha^* > 90°, f(\alpha^*) = 1$. According to Eqs. (34) and (35) there is a small change in τ_s if $\alpha^* < 22.5°$, then W_x decreases compared to the original value up to roughly 65°, followed by a relative increase and leading to a non-zero

value if $\alpha^* = 90°$. This transformation comprises the findings of Eqs. (1a) and (1b) but considering α^* as a continuous variable.

4.2. Model Calibration

The objective of this section is to determine the two most essential parameter values λ and C_D, respectively. For this purpose wind events of duration 2 and 12 h were selected. $|W|$ and α were systematically changed and the major results, I and Q, compared to Eqs. (1) and (2).

Figs. 13 and 14 give an indication of the influence of T. As can be seen, beside T = 12h, a larger denivellation results, as compared to T = 2h, but the further increase of T(e.g., a step-like wind input) does not now induce a higher fluctuation. For Q the maximal values are even equivalent for the three situations. After the decay of the wind, an abrupt change takes place in the water level. In accordance with the experiences, the second amplitude is approximately 30% of the first one, and one or two more significant amplitudes can be observed. This reasonable system behavior was achieved with bottom friction $\lambda = 0.003$, and drag coefficient $C_D = 0.0013$, both being realistic values. For the case set up the water surface approaches the steady state solution through small oscillations, while Q converges obviously in all three cases to zero.

The maximal denivellations as a function of W_x are given in Figs. 15 and 16 for the two different domains defined by Muszkalay (Section 2). His equations were transformed by assuming $W_{max}/\overline{W}_{max} = 1.2-1.3$ (see Section 2, item (ii)) and the corresponding ranges are illustrated. Bearing in mind the comments (i) - (vi) in Section 2 the model calibration is successfully performed for $|\alpha - 247.5| < 22.5°$. The model response is

acceptable also for the more transversal wind conditions (Fig. 16). Since the same W_x component can be realized by various (W, α) combinations, here the velocity isolines are indicated separately for $W_x = 8.12$ and 16m/s, respectively.

Fig. 17 shows that the saturation for I takes place at smaller value of T as contrasted to Eq. (1), a feature which was already observed in Fig. 13. Fig. 18 illustrates the comparison for the maximal discharge of stormy events. As a basis Eq. (2) was adapted by assuming $A = 4000m^2$ and $U = 0.8-1.0U^*$ (see Section 2). Fig. 18 shows that the (Q, I) domain derived from the model coincides satisfactorily with the empirical range based on Muszkalay's observations. With this final step, the calibration procedure ends. The validation of the model is discussed below.

5. MODEL VALIDATION

For the purpose of validation more than ten historical storms were selected from among Muszkalay's observations (Muszkalay 1973) and simulated under parameter values found in the previous section. The events chosen covered most of the possible stormy situations characterized by direction, speed, their changes, duration, etc. As input, hourly wind data measured at Szemes was used. The time step of the computation was 3600 s. For comparison, water levels observed at the two ends (Keszthely and Kenese) of the lake and discharge derived from velocity measurements at the peninsula (if they were available) were used. Subsequently, six examples will be discussed. The first two can be characterized by wind directions coinciding approximately with the axis of the lake,

the next three by perpendicular directions, while the last one consists of a set of subsequent, different events.

5.1. Event No. 1 (date: 16/11/1966, 8 a.m.)

The entire period covered a relatively long storm, when the wind blew from the east, followed by three smaller storms of various character (Fig. 19a). The corresponding wind shear stress pattern is illustrated by $F=W_x|W|$ in Fig. 19b. The shape of the water level is quite similar to that of the wind force and from this single example, a linear relationship between the two could be hypothesized. The maximum denivellation reaches 0.7 m, approximately one fourth of the average depth, one of the highest values observed. No second amplitude can be observed, which is mainly due to the gradual decay in the wind shear. The agreement between simulated and observed water levels is excellent. The discharge shows in the range (-2000; 3000 m^3/s) a highly fluctuating character. The mean value of the time series is negligible compared to the absolute values. During the first 25 hours of the storm more than $50.10^6 m^3$ water (nearly 10% of the volume of the Siófok basin) is transferred to the Szemes basin. This, however, does not mean the full mixing of this volume in the neighboring segment of the lake since the average distance travelled by a fluid particle is in the magnitude of 2-3 kms during the same event. Fig. 20a shows the entire solution z(t,x) in the three-dimensional space. This gives a higher visibility on the fluctuation of the free surface. The drastic change near the strait is especially apparent; an obvious consequence of the Venturi type structure here.

Fig. 20b includes the solution surface $Q(t,x)$. For the sake of better understanding, only a subdomain of $Q(t,x)$ was plotted, from Keszthely to Tihany in space, and 0-30 h in time. The figure clearly shows the role of the boundary condition and suggests at some time levels the existence of non-unidirectional flow. Some influences of the peninsula can also be observed. This is certainly much higher in terms of velocity.

5.2. Event No. 2 (date: 28/9/1965, 9 a.m.)

Compared to the previous example, there is a 180 ° shift in the wind direction (SW) with similar velocity values, thus resulting in the same order of magnitude for wind shear stress (Fig. 21, a and b). The event is like a storm surge with a duration of less than five hours, therefore the damping of the system can be better judged (Fig. 21c) than in the case of Event No. 1. The model captures reasonably well the water level motion except at the very beginning of the period for the eastern end of the lake. Here, most probably the wind set up started earlier and this fact is not reflected in the Szemes record. The discharge has a time pattern which is typical also for the rectangular wind input used for calibration. The agreement between the values gained from simulation and observation, respectively, is less satisfactory. This is, however, quite obvious, since (i)only a single point measurement was available; (ii) this is affected quite a bit in the vicinity of the peninsula by local phenomena (both in the atmosphere and water,) and (iii) for sensitivity reasons the proper simulation of the velocity is more difficult than that of the water level (a general feature of hydrodynamic models). Basically the description of the first peak in $Q(t)$ is successful (Fig. 21d), while the second is overes-

timated. During the subsequent period the noisy behavior of the discharge is apparent both, for simulation and observation.

5.3. Event No. 3 (date: 19/9/1965, 8 a.m.)

The wind direction is practically constant, NEN, and consequently the longitudinal component of the shear stress is smaller than before ,although the magnitude of the velocity is unchanged (Fig. 22, a and b). The duration of the storm is again long, nearly two days. As is clearly visible, the water level (Fig. 22c) sinks initially at the eastern end of the lake. This is then not followed by a usual seiche type oscillation; the renewed increase in the wind shear stress around t = 20 h prohibits a positive amplitude and forms a second "ebb"at Kenese. The simulation results for this location (no data were available for Keszthely) are quite appropriate except for the period t = 10 - 25h where the computation shows more pronounced changes than the observations. The uncertainty in the wind direction could be one reason (see below). For the discharge, the simulation follows the time pattern of measurements, however, the latter results in higher positive and negative flows (Fig. 22d).

5.4. Event No. 4 (date: 8/7/1967, 11 p.m.)

The storm is characterized by a northern wind blowing for more than two days (Fig. 23a). As with previous experiences, the shape of F(t) (see Fig. 25b) is well reflected in the pattern of the water level. As can be seen, the agreement between simulation and observation (Fig. 23c) is acceptable, although the latter shows more random influences. The discharge at the Strait shows the typical fluctuating character (Fig. 23d).

- 34 -

The sensitivity due to possible spatial changes in α is illustrated in this example (see 4.1.5 (ii)). A linear longitudinal variation was assumed in harmony with Section 2, defined by a small difference, 12°, between the two ends of the lake. As a result of this, an additional wind force is introduced, which is negative at the western part of the lake and positive from the midpoint towards the east. The solution turns out to be very sensitive on this minor modification (Fig. 24). The water surface becomes curved and at both ends of the lake mainly positive water level deviations can be observed. Simulation and observation do not show similarities at all: a clear indication that for cross blowing winds, small changes in the wind field can lead to unacceptable simulation results (see later).

5.5. Event No. 5 (date: 8/7/1963, 8 a.m.)

A typical situation for the lake: a strong wind perpendicular to the axis (Fig. 25a) resulting in a relatively small longitudinal shear stress component. The behavior of the water level is entangled enough (the changes are small and random) and the observed discharge shows much higher fluctuations than in the simulations, e.g., when the model fails, which is a consequence of the one-dimensional treatment and the uncertainties in the wind direction. The latter will be more closely examined in Section 6.

5.6. Event No. 6 (date: 18/4/1967, 2 p.m.)

The example represents the most comprehensive case, when within eight days more than five different situations covering the range 0-25 m/s and the complete domain of α can be distinguished, resulting in an irregular F(t) pattern (Fig. 26, a and b). From the comparison of the

observed and simulated water levels, the noisy character of the latter is apparent. When using moving averages for the computations a reasonable agreement is gained for the eastern end of the lake. The same is not true for Keszthely, the model gives an overprediction around t = 100h when the wind blows from the north. The discharge reflects the noisy character of the water level (which is valid for the entire free surface) and shows the largest oscillations among the examples discussed here.

5.7. Summary

The simulations introduced before support the calibration procedure adopted in Section 4 and also suggest an acceptable validation for longitudinal wind conditions. The model captures the major properties of the system for water level and to a somewhat lesser extent for the streamflow at the Tihany peninsula. This latter fact is also explained by the specific character of the observations. For cross wind conditions, the model performance is less satisfactory and may even fail. For this behavior, however, the uncertainties in the wind field are primarily responsible, an issue which will be discussed next.

6. UNCERTAINTIES RELATED TO WIND DIRECTION

Wind direction data are corrupted by various kinds of uncertainties. The most important error sources are the following:

(i) the improper registration and time averaging of the direction as a stochastic variable associated with turbulence. As a result of turbulent fluctuations, the continuous records often define a 40-60° wide domain rather than a single line (see Fig. 2);

- 36 -

(ii) the resolution of many instruments is discrete, 22.5° or sometimes even 45°;

(iii) the nonuniformity of the wind field (randomness in space) adds a further error component.Concluding from Section 2, this may exceed 90°.

In relation to item (i),for example, Gaussian distribution can be hypothesized. For situation (ii), α can take randomly three different values (the mean, ± 22.5 or $\pm 45°$). For the character of spatial randomness no information is available, thus the assumption of a uniform distribution is the most feasible.

In order to analyze the influence of the various kinds of uncertainties outlined in the model response, Monte Carlo simulations were performed. In the course of these a random component, α', is added to the mean value $\bar{\alpha}(t)$ ($\bar{W}(t)$ is unchanged). The generation of α' takes place numerically. Thus, theoretically, an infinitely large number of $\alpha_i = \bar{\alpha} + \alpha'_i$ scenarios can be produced, serving as input to the model. Selecting a sufficiently large number of such scenarios the model is run with them and the statistics of the output are evaluated. Here the three distributions (with zero means) mentioned before were realized for α'. In option (iii) the range can change with time, which corresponds to a situation when α is sampled randomly from a domain specified by records $\alpha_1(t)$ and $\alpha_2(t)$ taken at two different locations.

Four events were chosen for the purpose of the uncertainty analysis, Nos. 1, 5, and 6 already discussed in the previous section and the storm shown in Fig. 2 (13/7/1961) for which data were available for Keszthely

and Siófok. Simulations were performed with the various distributions by changing their major parameters as well. As basic, realistic parameters 16.8°, 22.5°, and 33.8° were assumed for the standard deviation and half-ranges (items (ii) and (iii)), respectively. After a set of test examples the number of simulations within a Monte Carlo run was fixed at 100. The transformation of the original distribution to wind force and then to water level and discharge, respectively, was also studied. Subsequently some of the results are separated.

6.1. Event No. 1

Figure 27 corresponds to Figure 19 involving means, ± standard deviations and envelopes for the wind force, water level at Keszthely and discharge, respectively. As is apparent, the uncertainty in α (uniform distribution, range 67.5°) influences only to a small extent the wind shear stress, as $|\alpha| = |\alpha^* - 247.5|$ is far from 90° and the cosine function is relatively insensitive here. As a consequence of this, z ranges also within a limited domain; around time t = 25 the standard deviation is practically zero. The uncertainty range of Q is essentially wider, indicating that model validation for the streamflow rate is more difficult than for water level. It is noted that the mean trajectories agree reasonably with the deterministic simulations (Fig. 19), furthermore, that the discrete generator (option (ii)) with 22.5° gave quite the same results as those illustrated in Figure 27.

6.2. Event No. 5

The results for rectangular distribution are given in Figure 28. In contrast to the previous example, the uncertainty resulted in F by the same range in α is much wider due to the cross wind conditions and the character of the cosine function. The water level can range between 0.15 and -0.15 m, thus covering all the observations. The results explain the noisy character of the water level and shows that under such conditions a deterministic model cannot be validated. For the discharge, a striking, broad domain was obtained, including most of the measurements. While in Section 5 it was said that the model failed for this event, from the present example it follows that this statement is true only if uncertainties are not accounted for.

Figure 29 summarizes the results gained with various distributions for the discharge at Tihany. It is stressed that the smallest uncertainty range is specified by Figure 29c, since the resolution of the standard wind direction data is 22.5°. From the plots and other examples of this section it follows that except longitudinal wind conditions the model is much more sensitive on α as input data than on model parameters: a fact which should be accounted for in model development and use.

As compared to the previous example, the mean trajectories depend much more on the distribution assumed for α and differ from the deterministic simulation.

6.3. Event No. 6

Results for the water level at the eastern end of the lake are given in Figure 30 (uniform distribution, 67.5° range). Attention is paid here on the mean trajectory rather than on the wide domain specified by the

envelopes. In essence the mean trajectory differs essentially from the deterministic result, it is much less noisy and agrees better with the observations.

6.4. Sampling α from the Domain Defined by Records of Two Stations

As mentioned before, the storm of 13/7/1961 (Figure 2) was simulated (the storm was one of the most violent observed since 1960). As wind velocity, the mean of the two measurements at Keszthely and Siófok, respectively was employed. The difference in direction moved around 30° when the highest absolute values took place. The envelopes of the Monte Carlo runs together with observations for the eastern end of the lake (hourly water level reading) are presented in Figure 31. For the sake of illustration, the continuous record (in a different scale taken from Muszkalay (1973)) is also given. The slightly broader domain of observations suggest among others a larger variation in α as specified by the two records.

At the end of this section it is noted that not only α but also W is a subject of various uncertainties. The influence of short-term fluctuations associated with turbulence was tested also in a Monte Carlo fashion by selecting small time steps (1-2 minutes), but no essential effect was observed. No further effort was made to analyze the influence of other types of uncertainty sources.

7. SIMULATION OF A COMPLETE YEAR: 1977

The year 1977 is the basic year for calibration of the lake eutrophication models in the frame of the Case Study (van Straten and Somlyódy, 1980). This is the reason for selecting this particular year here. As input, the record taken at Siófok (eight observations per day) was used with the appropriate selection of a_0 in Eq. (33). The time step of the computation and other parameter values remained the same as before.

Detailed results are presented for the streamflow rate in Figures 32 and 33 belonging approximately to the boundaries of basins and the midpoint of the Siófok basin, respectively (see Figure 1). January (Figure 32) was a month poor in wind, while during July (Figure 33) several big storms occurred (see Figure 33). The plots show the tendency expected on account of the previous experiences: fast dynamics and fluctuation on a wide range. Figure 32 illustrates clearly the longitudinal variation of Q-- small in the Keszthely region and the highest at Tihany. In July, the oscillation is stronger and Q ranges in the $\pm$ 3000 m^3/s domain for the eastern area of the lake.

A simple analysis of the hourly results underlines the major behavior of the system. Figure 34 shows the mean and standard deviation of the streamflow at Tihany on a daily basis throughout the whole year. It is apparent that the daily mean is smaller by approximately two orders of magnitude than the hourly values. This fact is also reflected in the high standard deviation. The peaks in the daily means are about ten times higher than the hydrologic throughflow, but for a longer time scale (e.g., a week) the mean of the dynamic flow is near zero. The influence of the discharge pattern derived on water quality is the next step of the analysis, as explained in the first section.

8. CONCLUSIONS

1. A one-dimensional, unsteady hydrodynamic model was developed and applied to Lake Balaton. The equation of motion and continuity was solved numerically by an implicit finite difference scheme. The system of linear equations gained was solved by a matrix sweep method (developed in the frame of this research) which is faster on the computer by two orders of magnitude than conventional techniques. The spatial stability was approved (the method is unconditionally stable in time).

2. The influence of the two major parameters, the wind drag and bottom friction coefficient, have opposite effects on the model performance. Thus, it is difficult to find a unique, "best" parameter combination. In the ranges $C_D = 0.0011 - 0.0014$ and $\lambda = 0.002 - 0.008$ fittings of approximately equal quality can be arrived at for I and Q. Based also on the damping properties of the system, a parameter vector (0.0013, 0.003) was concluded.

3. The model behavior is obviously sensitive to the drag coefficient (there is nearly a direct proportionality) influencing the energy input of the system. In contrast to this feature, the model output is quite insensitive to the bottom friction coefficient (the only parameter directly associated with internal variables). In the range of T related to the nominal value (0.25 - 8), I, the maximal denivellation of water surface during a storm changes in the +15 to -27% domain. The streamflow rate at a given cross section is slightly more sensitive, but both variables are practically independent of λ for $\lambda / \lambda_0 > 8$.

4. The model was successfully validated for longitudinal wind conditions (altogether six storms were simulated). The same is not quite true for winds closer to cross-direction and especially not for streamflow rate.

5. The reason for this failure is the uncertainty in the wind direction. The wind field is characterized by considerable temporal and spatial changes. While an error in the wind speed has a similar nature to that of the drag coefficient not influencing the direction of the flow or the sign of a water level amplitude, an error in the wind direction can completely distort the time pattern of the simulation. The response of the lake is very fast. A typical measure is the longitudinal seiche period, around ten hours according to the model. A storm of short duration (1-2 hours) induces considerable movement, thus a steady state practically cannot be defined. The resolution of wind data in time, space, and direction are not in harmony with the properties of the wind field and the fast dynamics of the system. The improper monitoring causes large uncertainties in the wind input data and should be accounted for in the course of model development.

6. This was done in Monte Carlo fashion. An error component sampled from a distribution (various distributions were used following the character of different error sources) was added to the mean scenario of wind direction, $\bar{\lambda}$ (t), and the model was run a sufficiently large number of times. The statistics of all the simulations were then evaluated.

Assuming realistic uncertainties in the wind direction (e.g., ±22.5 error domain) the model was successfully validated for all the historical storms simulated. The mean trajectories of Monte Carlo runs are close to

- 43 -

the deterministic simulations for longitudinal directions with increasing deviation towards cross-wind conditions.

7. In this particular case we can conclude that input data sensitivity dominates parameter sensitivity for the 1-D model. The pattern can certainly be different for other lakes. Still, it is generally of major importance to work out a proper wind monitoring network knowing the major features of the system in order to reduce the possible influences of input data uncertainties.

8. After calibration and validation, a complete year (1977) was simulated using observed wind data as input. The results showed the same striking pattern as that of the validation runs. The discharge ranges between $\pm 2-3000$ m^3/s, very high values (two orders of magnitude higher than the hydrologic throughflow). The flow changes, however, frequently change direction (roughly every 3 - 5 hours). For this reason the daily average discharge is much smaller (it moves in the +100, -100 m^3/s domain), associated with a 5 - 10 times higher standard deviation (both derived from the hourly values computed). The average of the streamflow on a longer time scale approaches zero. The influence of these pronounced dynamics on the ecology of the lake is to be studied with the help of a coupled biochemical-hydrophysical model.

APPENDIX I.   COEFFICIENTS OF THE FINITE DIFFERENCE EQUATIONS (21) AND (22)

$$A_{1i} = -2\,\vartheta\,\Delta t\,/\,\Delta x_i$$

$$A_{2i} = [B]_i^j$$

$$A_{3i} = 2\,\vartheta\,\Delta t\,/\,\Delta x_i$$

$$A_{4i} = [B]_i^j$$

$$A_{5i} = \frac{2\Delta t}{\Delta x_i}\,(Q_{i+1}^j - Q_i^j)$$

$$B_{1i} = \delta_4 Fr\left[\frac{1}{A}\right]_i^j - (\delta_2 + \delta_3)\,Fr\left[\frac{Q}{A^2}\right]_i^j\,\frac{2\vartheta\Delta t}{\Delta x_i} -$$

$$-\,(1 + n)\Delta t\,Fr\,\vartheta_1\,\frac{S_i^j}{Q_i^j}$$

$$B_{2i} = -\frac{2\vartheta\Delta t}{\Delta x_i\,Fr} + \delta_1\delta_2\,\frac{2\vartheta\Delta t}{\Delta x_i}Fr\left[\frac{Q^2}{A^3}\right]_i^j\,B_i^j +$$

$$+\,(2 + n)\,\Delta t\,Fr\,\vartheta_1\,\frac{S_i^j}{H_i^j}$$

$$B_{3i} = \delta_4 Fr\left[\frac{1}{A}\right]_i^j + (\delta_2 + \delta_3)\,Fr\left[\frac{Q}{A^2}\right]_i^j\,\frac{2\vartheta\Delta t}{\Delta x_i} -$$

$$-\,(1 + n)\Delta t\,Fr\,\vartheta_1\,\frac{S_{i+1}^j}{Q_{i+1}^j}$$

$$B_{4i} = \frac{2\vartheta\Delta t}{\Delta x_i\,Fr} - \delta_1\delta_2\,\frac{2\vartheta\Delta t}{\Delta x_i}Fr\left[\frac{Q^2}{A^3}\right]_i^j\,B_{i+1}^j +$$

$$+\,(2 + n)\Delta t\,Fr\,\vartheta_1\,\frac{S_{i+1}^j}{H_{i+1}^j}$$

$$B_{5i} = -\frac{2\vartheta\Delta t}{\Delta x_i Fr}\,(z_{i+1}^j - z_i^j) - (\delta_2 + \delta_3)\,Fr\left[\frac{Q}{A^2}\right]_i^j\,\frac{2\Delta t}{\Delta x_i}\,(Q_{i+1}^j - Q_i^j) +$$

$$+\,\delta_3\left[\frac{Q^2}{A^3}\right]_i^j\,Fr\,\frac{2\Delta t}{\Delta x_i}(A_{i+1}^j - A_i^j) + \Delta t\,Fr\,(S_i^j + S_{i+1}^j) +$$

$$+\,r_w\,2\Delta t\,Fr\left[\frac{1}{H}\right]_i^j\,W_x|W|$$

where $[f]_i^j = \frac{1}{2}(f_{i+1}^j + f_i^j)$ for any expression f, and $S_k^j = -\frac{r_b}{H_k^j}\,\frac{Q_k^j\,|Q_k^j|^n}{(A_k^j)^{n+1}}$

for $k = i$ and $i + 1$.

The matrix coefficients of Eq. (22) are

$$\mathbf{A_i} = \begin{bmatrix} A_{4i} & A_{3i} \\ B_{4i} & B_{3i} \end{bmatrix} \quad \mathbf{y_{i+1}} = \begin{bmatrix} v_{i+1} \\ u_{i+1} \end{bmatrix}$$

$$\mathbf{B_i} = \begin{bmatrix} -A_{2i} & -A_{1i} \\ -B_{2i} & -B_{1i} \end{bmatrix} \quad \mathbf{y_i} = \begin{bmatrix} v_i \\ u_i \end{bmatrix}$$

$$\mathbf{c_i} = \begin{bmatrix} A_{5i} \\ B_{5i} \end{bmatrix} \ .$$

APPENDIX II. STABILITY ANALYSIS FOR ERROR ACCUMULATION IN SPACE

II. A. The Basis for Analysis

When computing the relation between boundary values $\mathbf{y_1}$ and $\mathbf{y_N}$, and Eqs. (23) and (24), a round-off error $\mathbf{\varepsilon_i}$ may appear at any point i in the grid (i = 2, ..., N - 1). This error is then amplified by $\mathbf{A_k^{-1}B_k}$ matrices (k = i + 1, ..., N) to the end of the basin (i = N) to

$$\mathbf{\varepsilon_N} = \prod_{k=N}^{i+1} (\mathbf{A_k^{-1}B_k}) \, \mathbf{A_i^{-1}} \, \mathbf{\varepsilon_i} \ . \tag{II.1}$$

In order to obtain a stable solution with the desired accuracy $||\mathbf{\varepsilon_N}|| < \varepsilon$ the amplifying norm $||\mathbf{A_k^{-1}B_k}||$ must be sufficiently limited.

Since both $\mathbf{A_i}$ and $\mathbf{B_i}$ are 2 x 2 matrices only they should be inverted and multiplied analytically resulting in the amplification matrix $\mathbf{A_i^{-1}B_i}$. Furthermore, its eigenvalues λ_{i1}, λ_{i2}, and eigenvectors $[P_{i11}, P_{i12}]^T$, $[P_{i21}, P_{i22}]^T$ can be solved. Provided that

$$||\mathbf{P_i}|| \ ||\mathbf{P_i^{-1}}|| < K < \infty \tag{II.2}$$

for

$$\mathbf{P_i} = \begin{bmatrix} P_{i11} & P_{i21} \\ P_{i12} & P_{i22} \end{bmatrix}$$

the matrix $\mathbf{A_i^{-1}B_i}$ can be diagonalized to $\mathbf{\Lambda_i} = \left| \lambda_{i1}, \lambda_{i2} \right|$, Eq. (27). Its singu-

larities (locations of infinite matrix norm) then coincide with those of $A_i^{-1}B_i$ justifying the analysis of $||\Delta_i|| = \sqrt{\lambda_{i1}^2 + \lambda_{i2}^2}$ instead of estimation of $||A_i^{-1}B_i||$ from four nonzero elements.

Especially with matrix elements constant in space the diagonalization is attractive since then $P_i = P_{i+1} = \cdots = P_N$ and the matrix product (II.1) is simplified to

$$\mathcal{E}_N = P_N \begin{bmatrix} \lambda_{i1}^{N-1} & 0 \\ 0 & \lambda_{i2}^{N-1} \end{bmatrix} P_{i+1}^{-1} A_i \mathcal{E}_i . \tag{II.3}$$

However, also with nonconstant coefficients the analysis of $||\Delta_i||$ is exact as far as singularities are considered and as far as (II.2) is valid.

II. B. The Eigenvalues and Diagonalization

The matrix elements of A_i and B_i (Appendix I) contain a lot of common or closely similar terms. Thanks to their similarity the diagonalized matrix norm $||\Delta_i||$ can be derived with moderate assumptions (see Section II.E) to

$$||\Delta_i|| = \sqrt{2 \frac{1 + 6\overline{w} + \overline{w}^2 + \overline{e}^2}{(1 - w + e)^2}} \tag{II.4}$$

where

$$w = C_i^2 \frac{1 - \delta_1 \delta_2 F_i^2}{\delta_4 + (n+1)R_i C_i} \tag{II.5}$$

$$e = C_i F_i \frac{\delta_2 + \delta_3 + (n+2)R_i C_i}{\delta_4 + (n+1)R_i C_i}$$

and further

$$C_i = \frac{2\vartheta \Delta t}{\Delta x_i} \frac{\sqrt{H_{i+1}}}{Fr}$$

$$F_i = Fr\, U_{i+1} / \sqrt{H_{i+1}} \tag{II.6}$$

$$R_i = \vartheta_1 r_b |U_{i+1}|^n \frac{\Delta x_i\, Fr}{2\vartheta H_{i+1}\sqrt{H_{i+1}}} .$$

Parameters δ_k (k = 1, ..., 3) are the known switching coefficients for the three nonlinear effects, δ_4 is the same for local acceleration $\partial Q / \partial t$ and n is the bottom friction exponent as defined in Chapter 3.1.

C_i can be characterized as the Courant number of gravity waves in the grid, F_i as the local Fronde number, and R_i as the relative friction resistance. For stability analysis it is attractive that Δt appears in C_i only and r_b just in R_i. In (II.6) the velocities U and depths H are taken from cross section i + 1 since these appear in the elements of $\underline{A}_i$ which is to be inverted. Therefore they are essential to the singularities. The approximations needed for (II.4) - (II.6) and their influence will be analyzed in greater detail in Section II.E.

For a $\underline{P}_i$ matrix the following is obtained

$$||\underline{P}_i|| \ ||\underline{P}_i^{-1}|| \leq 1 + \frac{|\ \dfrac{2\vartheta\Delta t}{[B]_i^j \Delta x_i} - w\ \dfrac{[B]_i^j \Delta x_i}{2\vartheta\Delta t}\ |}{\sqrt{e^2 + 4w}} \ . \tag{II.7}$$

If this upper limit satisfies (II.2) the diagonalization indicated in Eq. (27) is justified and the analysis of singularities can be based on (II.4).

II. C. Linear Stability Conditions

Assuming first the linear case $\delta_1 = \delta_2 = \delta_3 = n = 0$ and coefficients constant in space $f_i = [f]_i^j = f_{i+1}$ (f = A, B, H, U, Q, etc.) four different sub-cases are to be distinguished according to the denominator terms in (II.4):

1° $\delta_4 = 0$, $r_b = 0$

(frictionless diffusive wave)

$2°$ $\delta_4 = 1$, $r_b = 0$ (frictionless motion with local acceleration)

$3°$ $\delta_4 = 0$, $r_b > 0$ (diffusive wave with friction)

$4°$ $\delta_4 = 1$, $r_b > 0$ (full solution with friction).

In each of them slightly differing matrix norms and stability conditions are obtained.

In case $1°$ ($\delta_4 = R_i = 0$) the diagonalization is not allowed by (II.7), (II.2) and the matrix norm will be estimated directly from

$$A_i^{-1}B_i = \begin{bmatrix} 1 & 0 \\ -\dfrac{[B]_i^j \Delta x_i}{\vartheta \Delta t} & 1 \end{bmatrix} \text{ leading to}$$

$$||A_i^{-1}B_i|| = \left[2 + \left(\frac{[B]_i^j \Delta x_i}{\vartheta \Delta t} \right)^2 \right]^{\frac{1}{2}} \tag{II.8}$$

(with the Eulerian definition of matrix norm). Small values of Δt and ϑ are detrimental to stability. The desired accuracy $||\underline{\varepsilon}_N|| < \varepsilon$ can be achieved only if the upper limit for initial error ε_0 is sufficiently limited so that $||\underline{\varepsilon}_i|| < \varepsilon_0 < \varepsilon / \sqrt{2^{n-1}}$. Necessary conditions for stability is then

$$\vartheta \, \Delta t > \frac{[B]_i^j \max \Delta x_i}{\sqrt{(\varepsilon / \varepsilon_0)^{\frac{2}{N-1}} - 2}} \, . \tag{II.9}$$

In cases $2°$, $3°$, and $4°$ the diagonalization is justified ((II.7) limited) and the stability properties are described by the diagonalized matrix norm (II.4).

Case by case, the singularities are located at

$$C_i = 0 \text{ in case } 1° \tag{II.10}$$

at

$$C_i = 1 \text{ in case } 2° \tag{II.11}$$

at

$$C_i = \frac{(n + 1) R_i}{1 - (n + 2) R_i F_i} \quad \text{in case } 3^\circ \qquad (II.12)$$

and at

$$C_i = \frac{(n + 1) R_i \pm \sqrt{(n + 1)^2 R_i^2 + 4\delta_4 [1 - (n + 2) R_i F_i]}}{2[1 - (n + 2) R_i F_i]} \qquad (II.13)$$

in case 4°.

In case 2° both high $(C_i > 1)$ and low $(0 < C_i < 1)$ values keep the matrix norm limited. The same applies to cases 3° and 4° but for these the critical values (II.12), (II.13) are no more defining a single point since F_i varies with velocity U_{i+1}. Positive values of U_{i+1} are the most restrictive to large time-steps and negative velocities to small values of C_i. Between these bounds instability occurs if U_{i+1} happens to have a value closely satisfying (II.12) or (II.13), respectively. Outside this region ("zone of instability") the solution is always numerically stable.

The behavior of matrix norms (II.8) and (II.4) are illustrated in Figures 6a-d.

II. D. Nonlinear Stability Conditions

1. Nonlinear bottom friction $(n > 0)$ makes the friction resistance R_i depend on velocity U_{i+1}. Thus the zero friction effect $R_i = 0$ is obtained not only by $r_b = 0$ (or $\vartheta_1 = 0$) but also with $U_{i+1} = 0$; so the singularities of cases 1° and 2° must be included in the "unstable zone" of cases 3° and 4°, respectively. As a consequence of this the small values of C_i will no more be acceptable in case 3° even in theory. This is also indicated in Figure 6c.

2. Explicit nonlinearities ($\delta_i = 1$, $i = 1, 2, 3$,) do not impend the diagonalization in cases $2°$, $3°$, and $4°$, so Eq. (II.4) is still valid for them. In case $1°$ the direct estimation of Eulerian matrix norm now results in

$$||A_i^{-1}B_i|| = \left[2 + \frac{\left[\dfrac{[B]_i^j \Delta x_i}{\vartheta \, \Delta t}\right]^2 + 4 \dfrac{\delta_2 + \delta_3}{1 - \delta_1\delta_2 F_i^2} \dfrac{F_i}{C_i}}{\left[1 - \dfrac{\delta_2 + \delta_3}{1 - \delta_1\delta_2 F_i^2} \dfrac{F_i}{C_i}\right]^2}\right]$$ (II.14)

The singularities are located at the solutions for equation

$$[1 - (n + 2)R_iF_i - \delta_1\delta_2F_i^2]C_i^2 - $$
$$[(n + 1)R_i + (\delta_2\delta_3)F_i]C_i - \delta_4 = 0$$ (II.15)

which is a general expression including - as its special applications - the singularities (II.10) - (II.13) as well as the singularity of (II.14).

The formal solution of (II.15) with nonlinearities will be more or less similar to (II.13). Thus in principle nothing new is brought to the stability properties by the explicit nonlinearities. As a detail, parameter δ_1 has no effect if $\delta_2 = 0$, as can be seen from Eqs. (II.5) and (II.15).

The zone of possible instability will be widened by the nonlinearities but outside the immediate vicinity of singularity points their effect on the amplifying matrix norm (II.4), or (II.14) versus (II.8), is less than or approximately equal to 10 per cent.

II. E. Stability Conditions under Space Gradients

Among the elements of A_i and B_i (Appendix I) there were terms from cross section i and i + 1 as well as their averages. In the previous analysis they were all assumed to be equal. Full attention to the space gradients will considerably complicate the expressions, though the basic definitions

of C_i, F_i, R_i, see (II.6), remain unchanged. Expressions (II.4), (II.5) are now replaced by

$$A_i^{-1}B_i = \tag{II.16}$$

$$\frac{1}{1-w+e}\left[\begin{array}{cc} -1-w-e-\Delta_2 & \dfrac{C_iFr}{[B]_i^j\sqrt{H_{i+1}^{--}}}(2+\Delta_1) \\[3mm] \dfrac{[B]_i^j\sqrt{H_{i+1}^{--}}}{C_iF_r}(2+\Delta_2)W & -1-w+e-\Delta_1 \end{array}\right]$$

where

$$w = C_i^2\left[1 - \delta_1\delta_2F_i^2\ \frac{[Q^2/A^3]_i^j}{Q_{i+1}^2/A_{i+1}^3}\right]\frac{1}{D_i} \tag{II.17a}$$

$$e = C_iF_i\left[(\delta_2+\delta_3)\ \frac{H_{i+1}[B]_i^j[Q/A^2]_i^j}{Q_{i+1}/A_{i+1}} + (n+2)R_iC_i\right]\frac{1}{D_i} \tag{II.17b}$$

with the common denominator D_i and the special shifting terms Δ_1, Δ_2

$$D_i = \delta_4\ H_{i+1}[B]_i^j\left[\frac{1}{H}\right]_i^j + (n+1)R_iC_i\ \frac{[B]_i^j}{B_{i+1}} \tag{II.18a}$$

$$\Delta_1 = (n+1)R_iC_i\ \frac{Fr[B]_i^j}{B_{i+1}}\left\{\frac{|Q_i/A_i|^n}{|Q_{i+1}/A_{i+1}|^n}\ \frac{H_{i+1}A_{i+1}}{H_iA_i} - 1\right\}$$

$$\Delta_2 = \frac{C_i^2F_i}{D_i}Fr\left\{-\delta_1\delta_2\ \frac{[Q^2/A^3]_i^j}{Q_{i+1}^2/A_{i+1}^3}\left[\frac{B_i^j}{B_{i+1}^j} - 1\right]\right\} + \tag{II.18b}$$

$$+ (n+2)R_i\left[\frac{\dfrac{Q_i}{A_i}|Q_i/A_i|^n}{\dfrac{Q_{i+1}}{A_{i+1}}|Q_{i+1}/A_{i+1}|^n}\ \frac{H_{i+1}^2}{H_i^2} - 1\right]\right\}.$$

Note that if space gradients are neglected, expressions (II.4) - (II.5) result in

$$\left\{1 - (n+2)R_iF_i - \delta_1\delta_2F_i^2\ \frac{[Q^2/A^3]_i^j}{Q_{i+1}^2/A_{i+1}^3}\right\}\ C_i^2 -$$

$$-\left\{ (n + 1)R_i \frac{[B]_i^j}{B_{i+1}} + (\delta_2 + \delta_3)F_i \frac{[Q/A^2]_i^j [B]_i^j H_{i+1}}{Q_{i+1}/A_{i+1}} \right\} C_i - \qquad (II.19)$$

$$-[B]_i^j \left[\frac{1}{A}\right]_i^j H_{i+1}\delta_4 = 0 \ .$$

From Eq. (II.19) it is clear that a) without nonlinear terms the space gradients are not very important (factors $[B]_i^j / B_{i+1}$ and $[B]_i^j \left[\frac{1}{A}\right]_i^j H_{i+1}$ only) but that b) a multiple effect of nonlinearities (a factor of $\frac{[Q^2/A^3]_i^j}{Q_{i+1}^2 / A_{i+1}^3}$) is gained by the space gradients.

Despite the rather strong influence of space gradients on certain single terms the principal nature and behavior of the amplifying matrix norm do not fundamentally diverge from that shown in Figure 6.
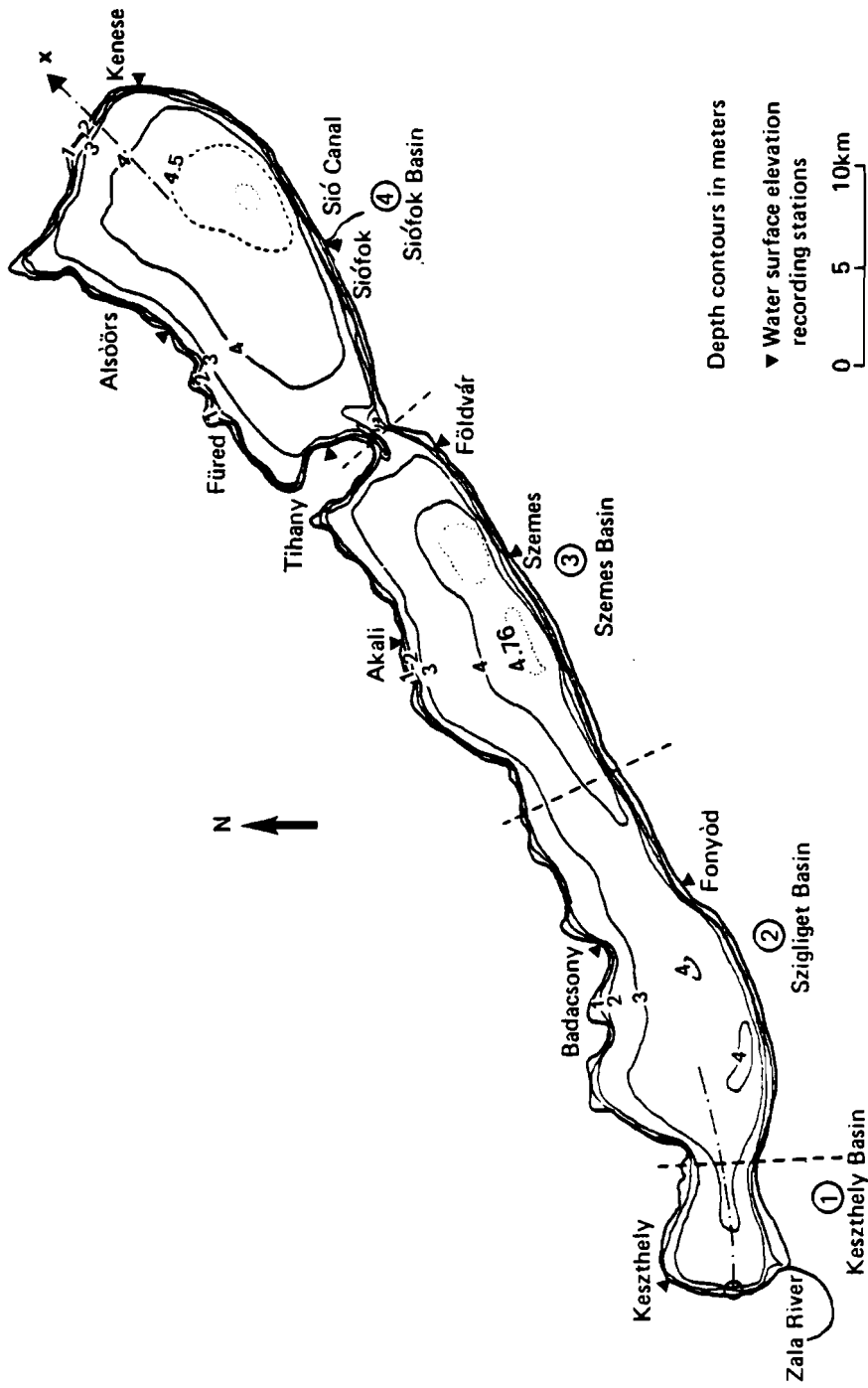
Figure 1. Major characteristics of Lake Balaton
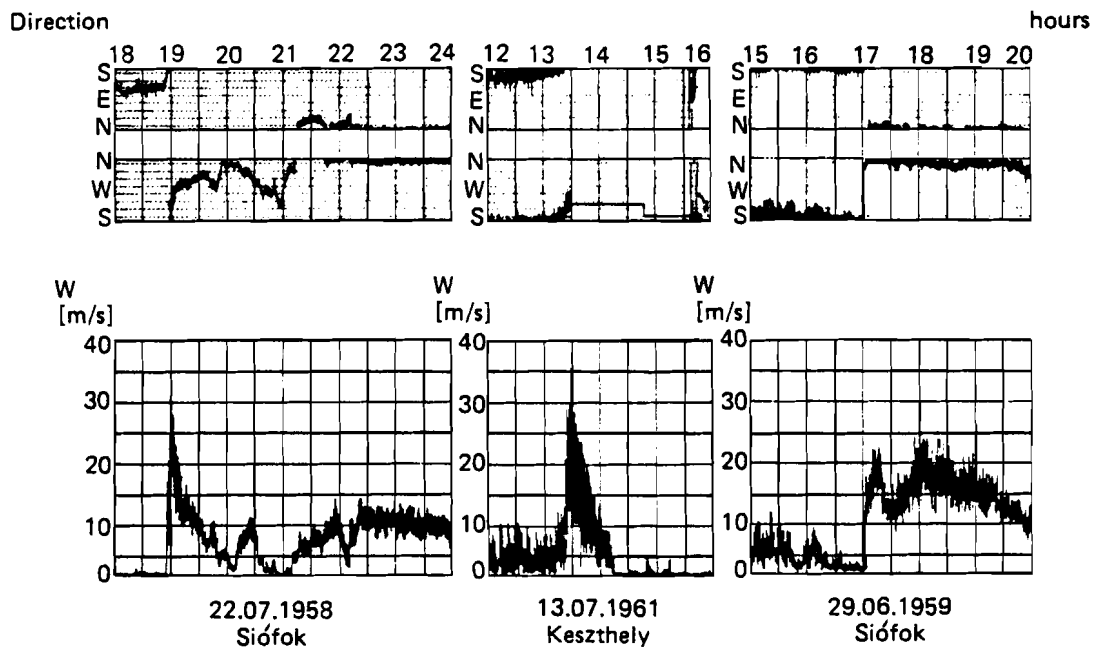
Figure 2. Typical stormy events (taken from Béll and
            Tabács, 1974)

-55-
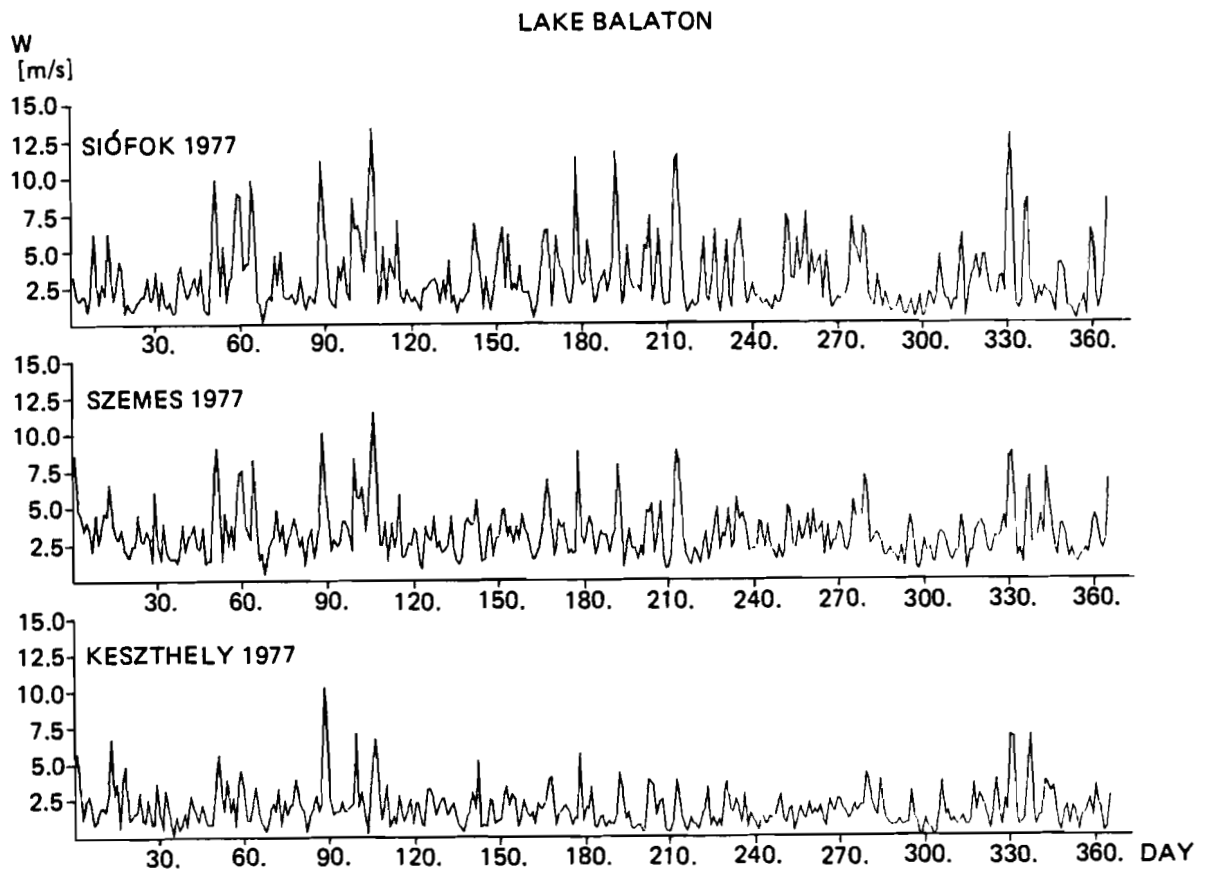
Figure 3. Wind record for three stations close to the lake
        (daily averages)

LAKE BALATON
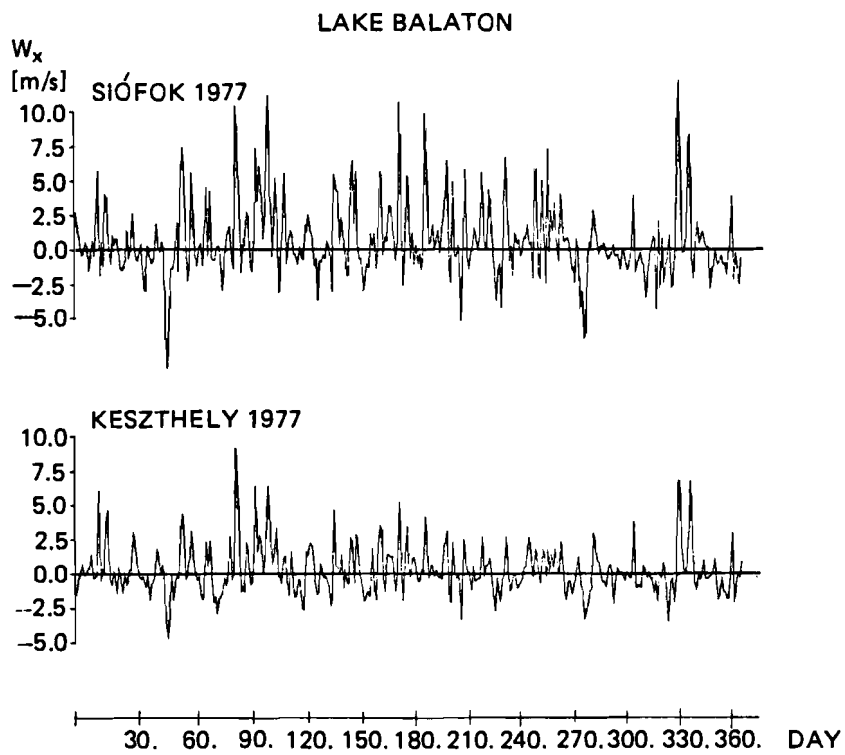
Figure 4. Longitudinal component of the wind velocity
vector for Siófok and Keszthely
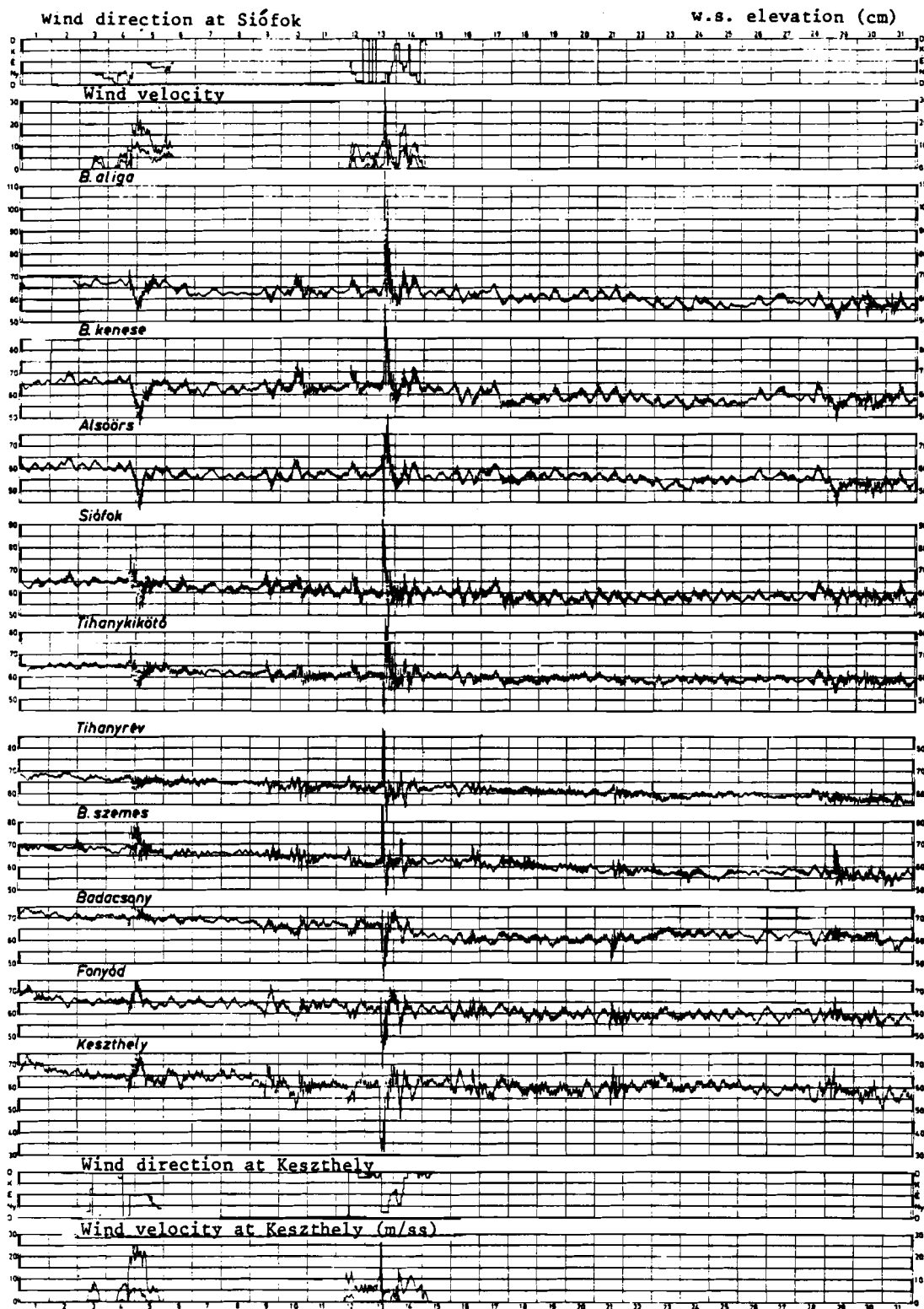
Figure 5. Typical water level records at various stations along the lake (see Figure 1) (taken from Kuszkalay, 1973)
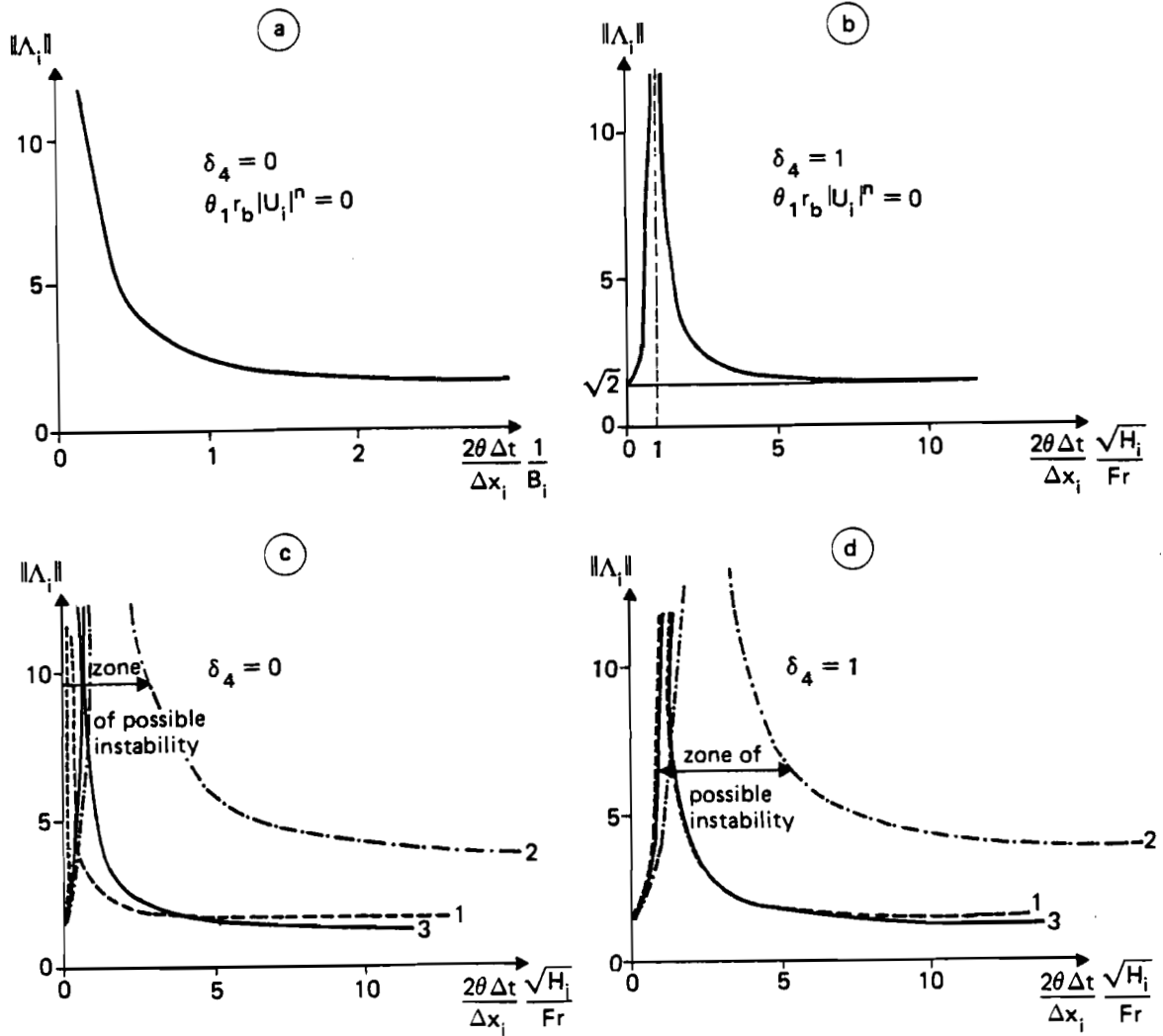
Figure 6. Results of the stability analysis i norm
of the amplification matrix
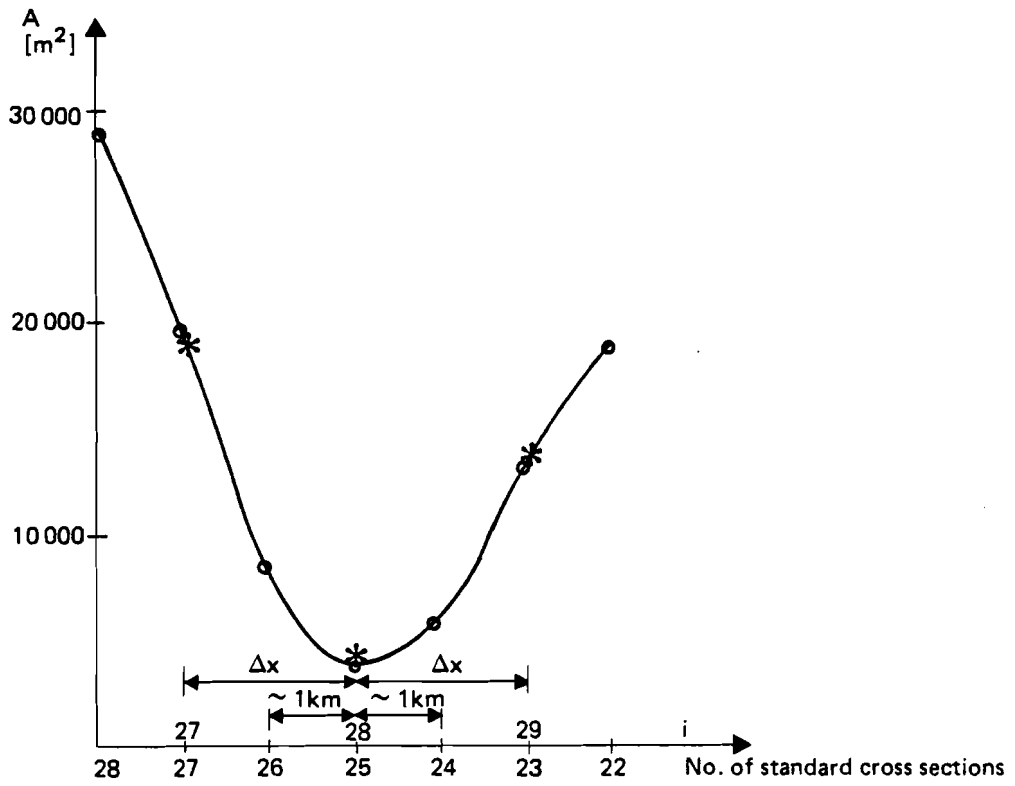
Figure 7.   The change in cross-section area in the vicinity of the peninsula
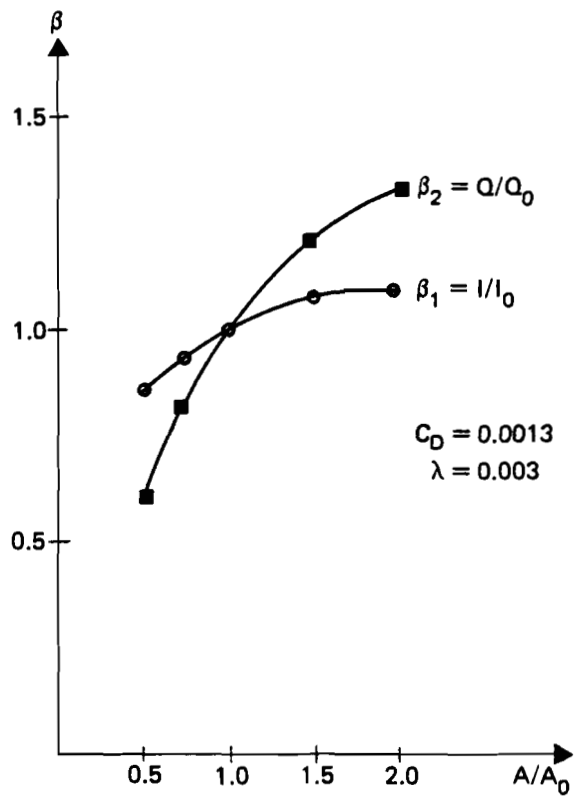
Figure 8. Sensitivity of the model on the smallest
cross-section area at the Strait
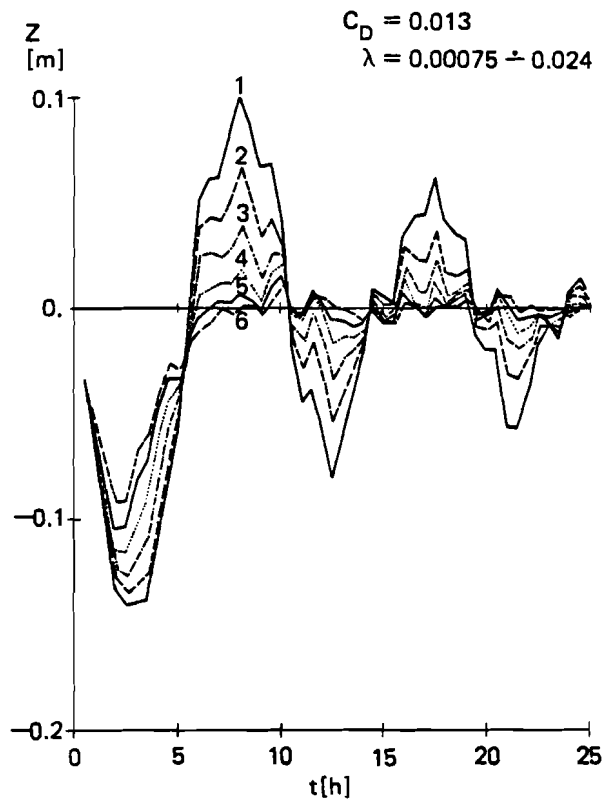
Figure 9. Water level oscillation at Keszthely besides
various bottom friction coefficients
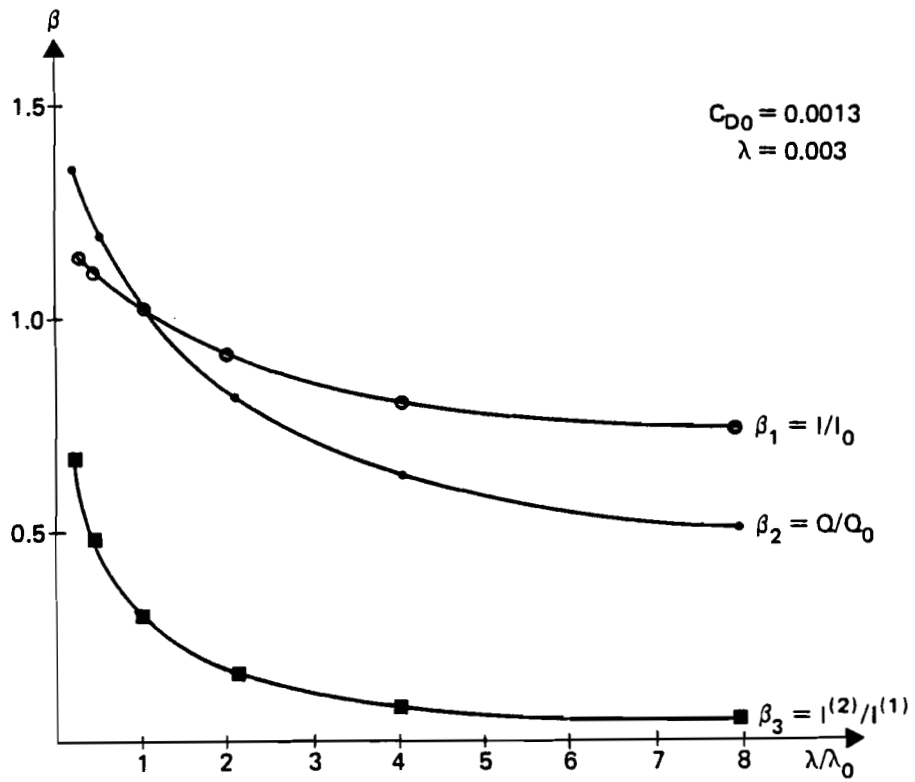
Figure 10. Model sensitivity on the bottom friction
coefficient
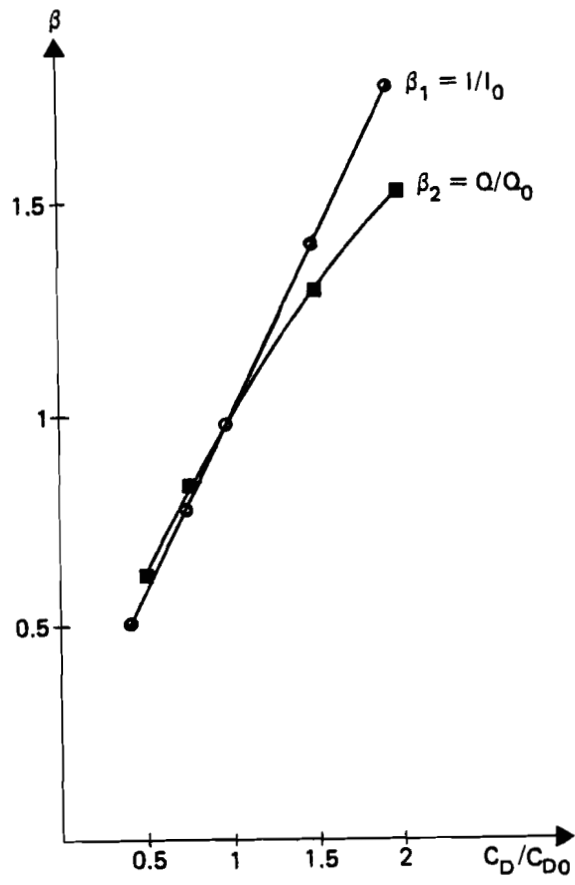
Figure 11. Model sensitivity on the wind drag coefficient
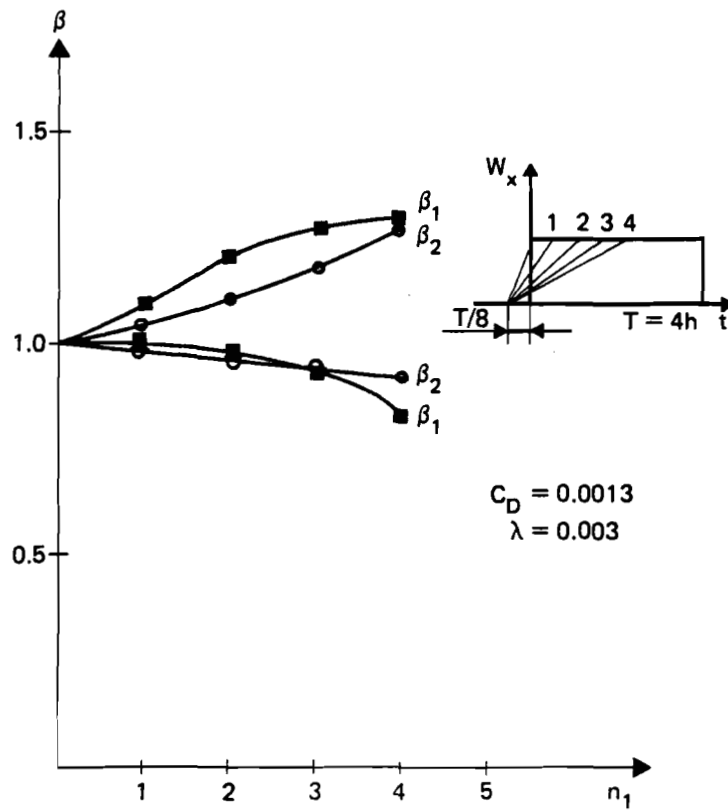
Figure 12. Model sensitivity on the shape of the wind profile
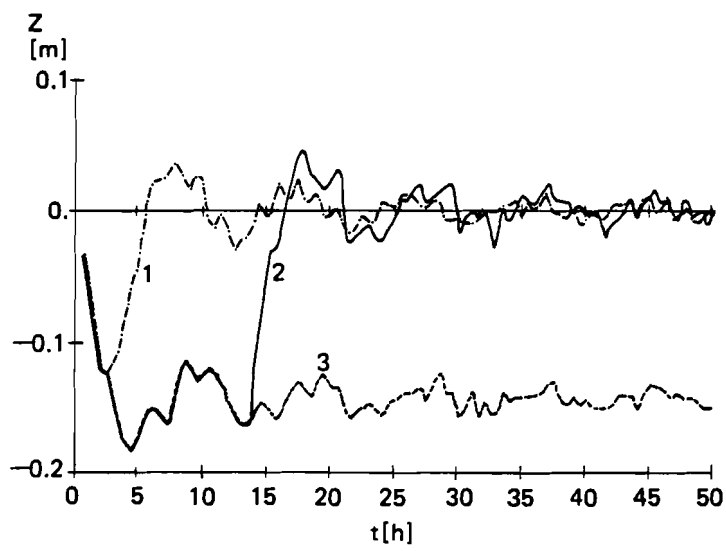
Figure 13. The influence of the wind duration on water
level oscillation
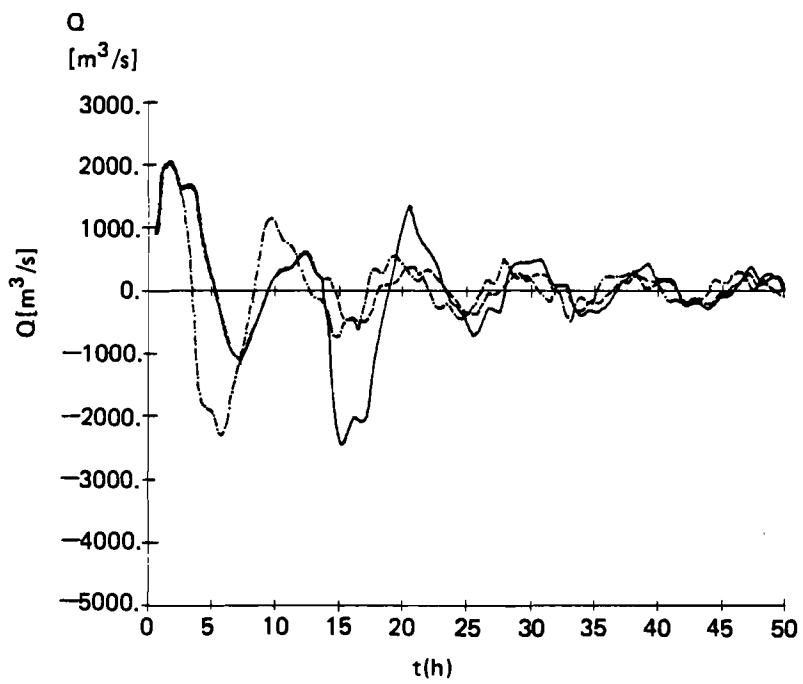
Figure 14. The influence of the wind duration on the
streamflow at Tihany
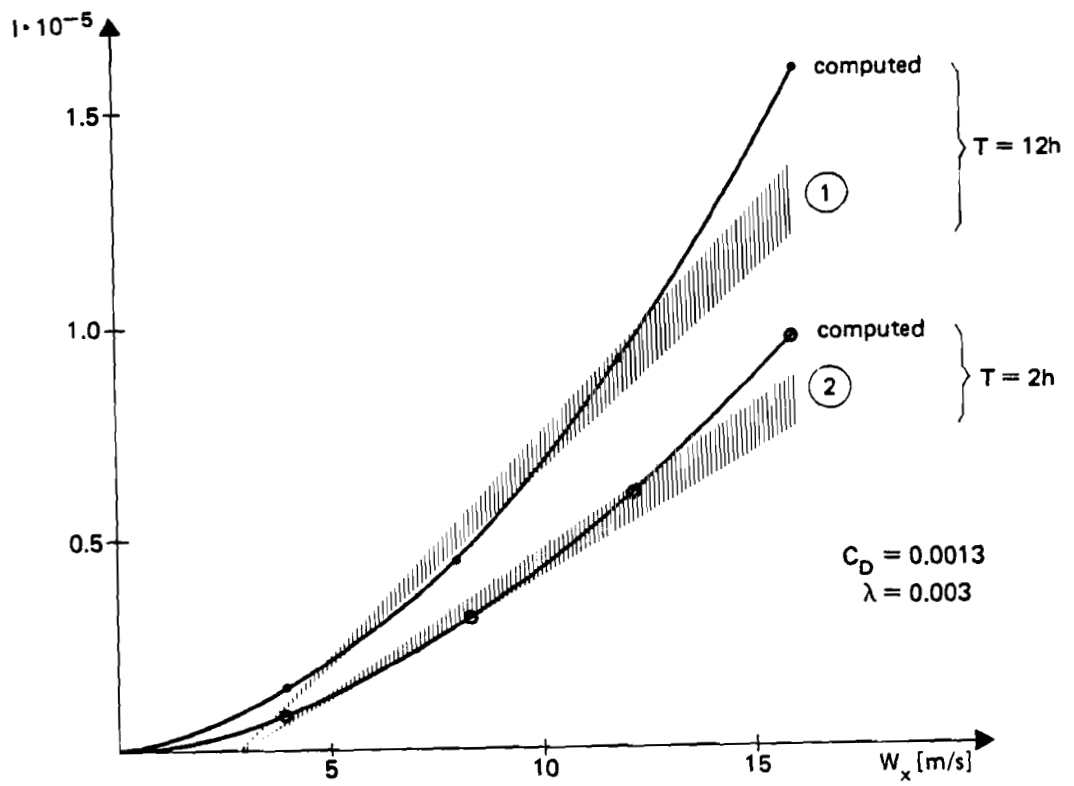
Figure 15. The maximal denivellation as a function of
W_x, $|\alpha - 247.5| < 22.5^\circ$
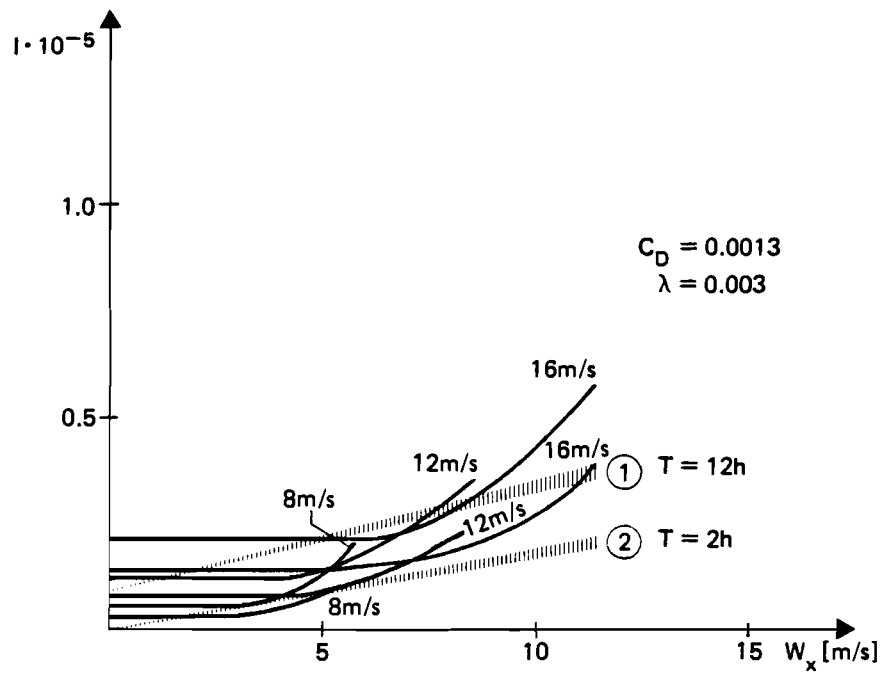
Figure 16. The maximal denivellation as a function of W_x
$|\alpha- 247.5^o| \geq 22.5$
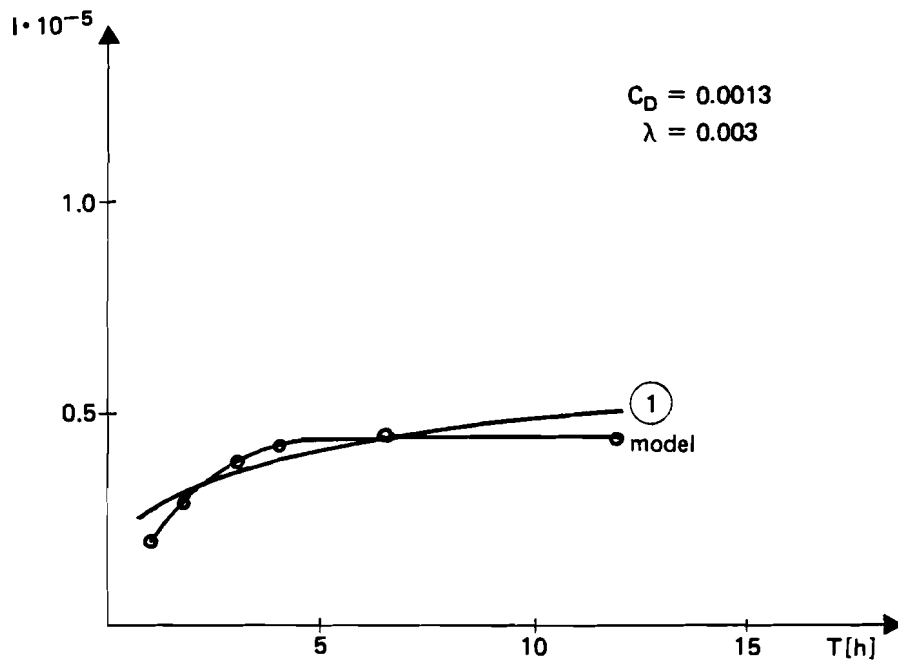
Figure 17. The change of the maximum denivellation as
          a function of wind duration
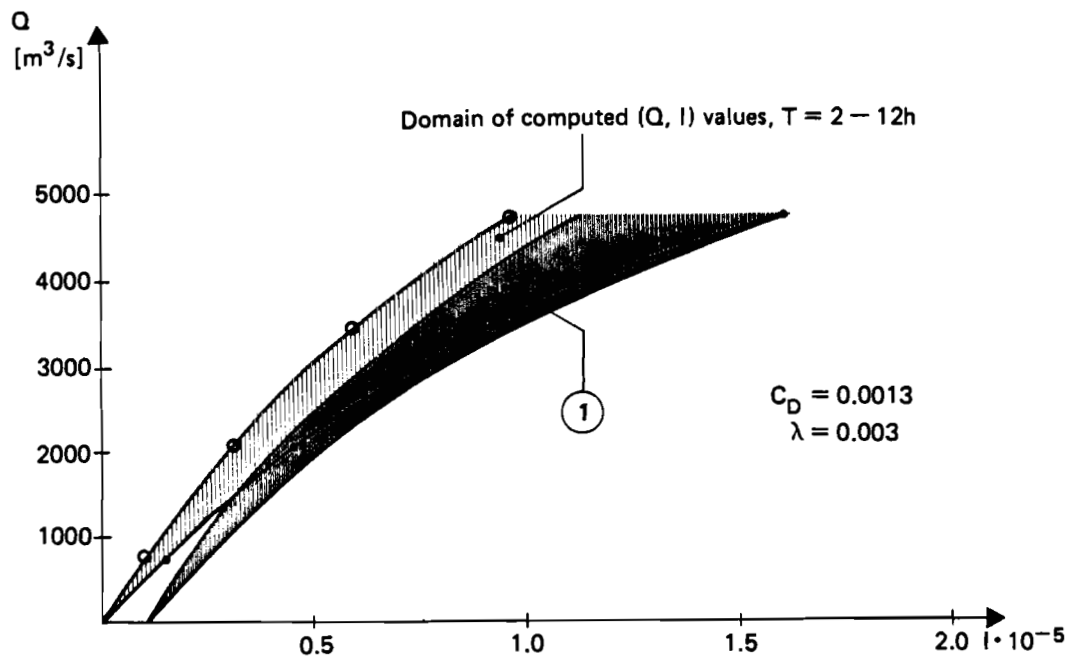
Figure 18. Comparison of discharges derived from observations, ①, and computations, respectively
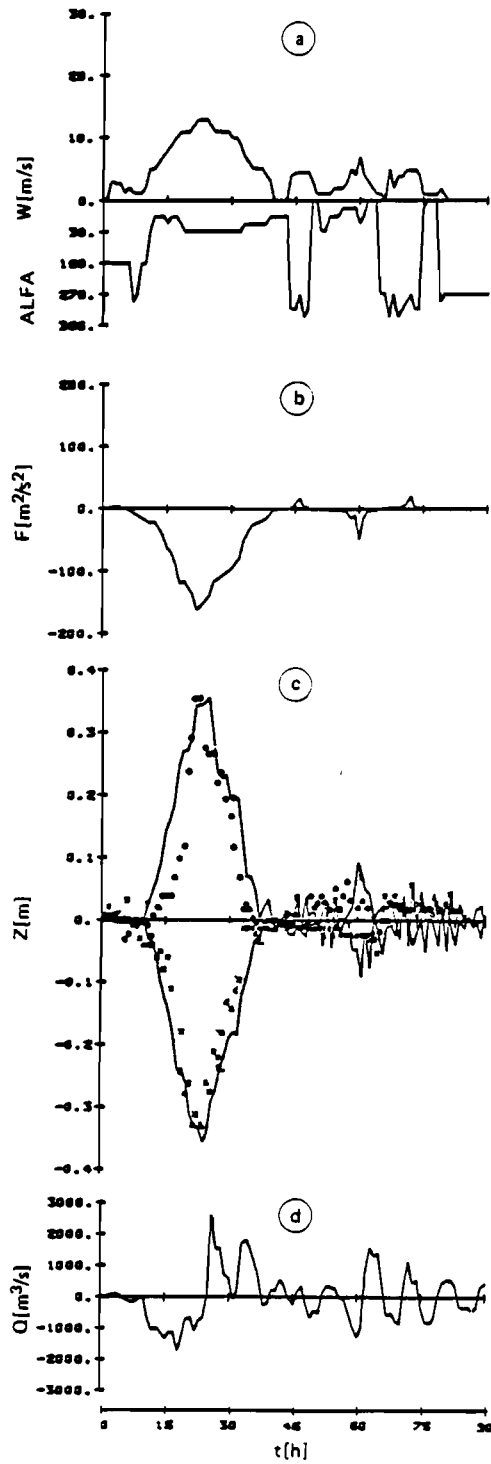
Figure 19. Simulation of a historical storm, 16.11.1966
        a) Wind speed and direction at Szemes,
        b) $F = |W|W_x$, c) Water level at Keszthely (1)
        and Kenese (2) together with observations,
        d) Discharge at Tihany
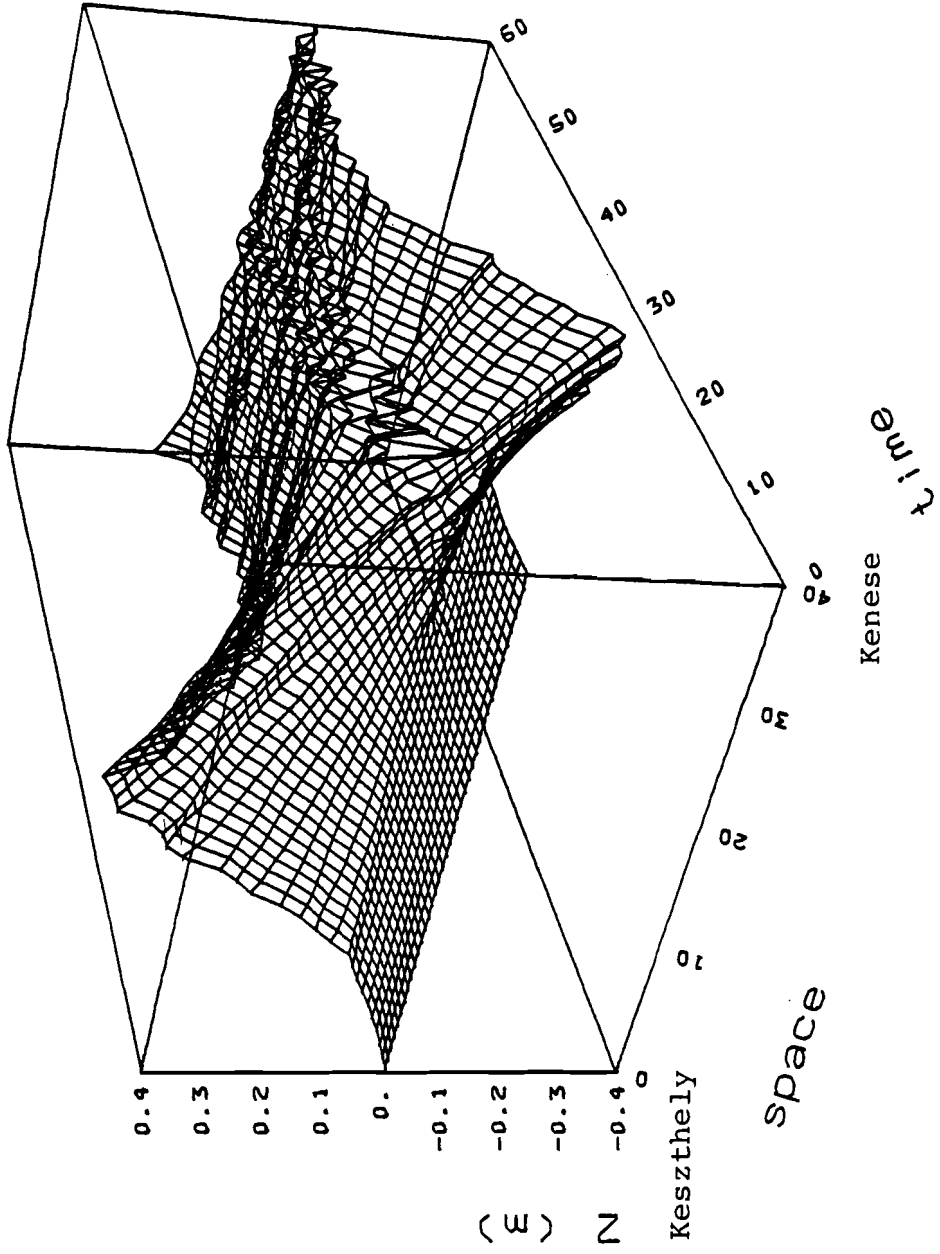
Figure 20a. Fluctuation of the water surface during the storm of 16.11.1966

Lake Balaton
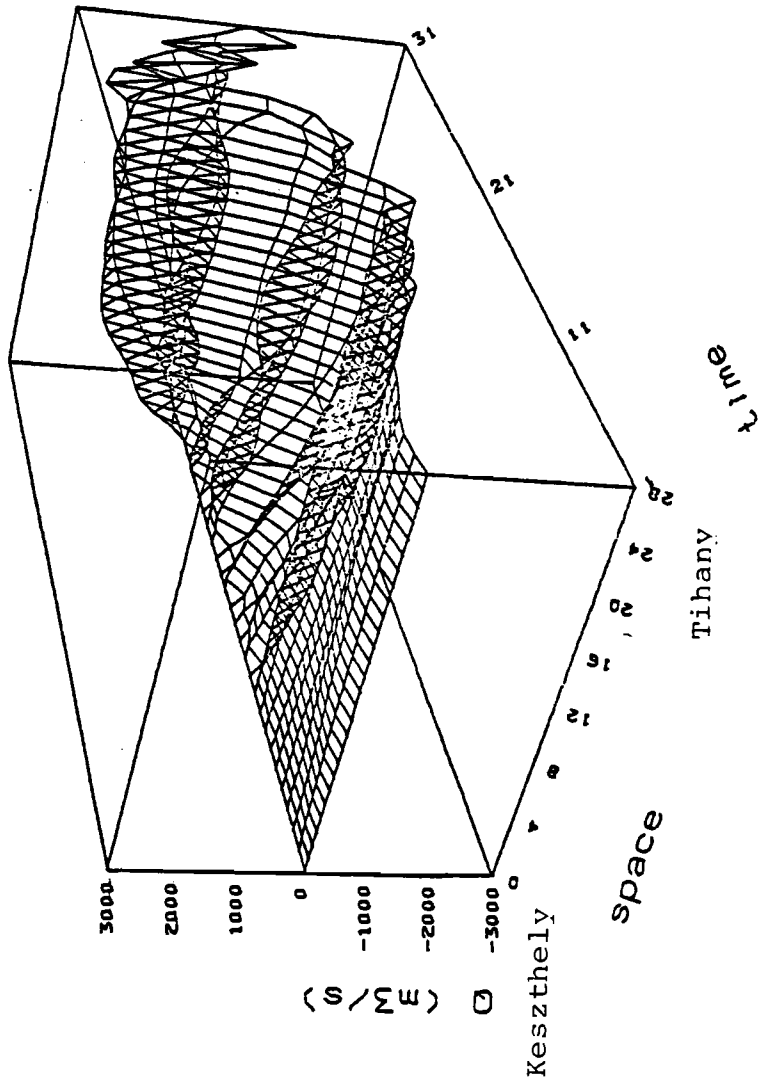
Figure 20b. Solution surface for the discharge, 16.11.1966

-74-
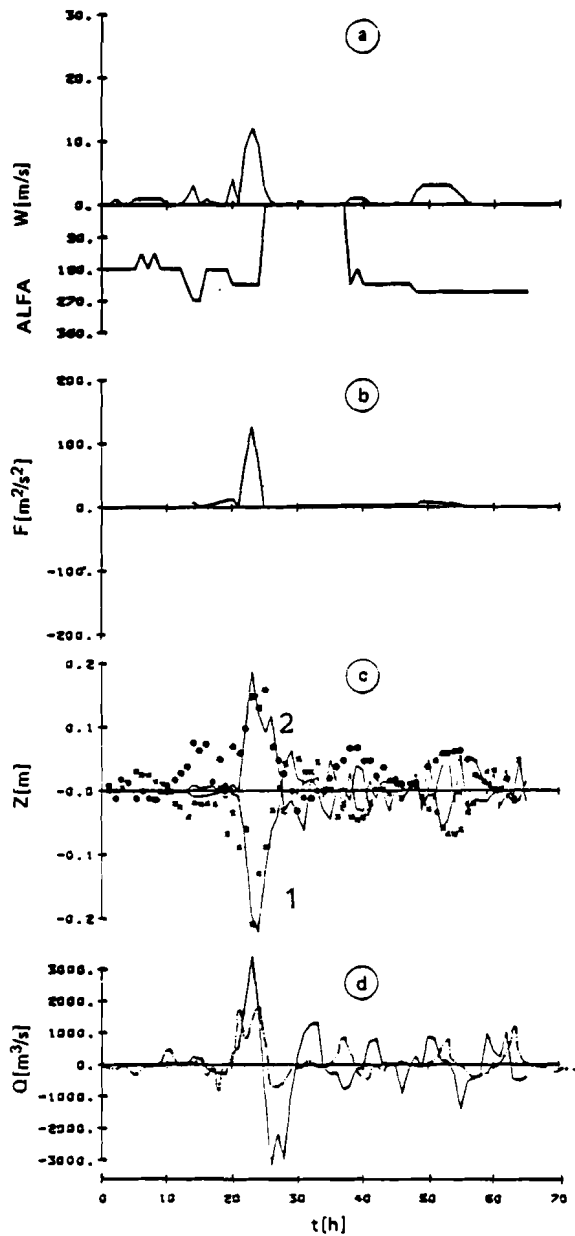
Figure 21. Simulation of a historical storm, 28.9.1965
   a) Wind speed and direction at Szemes,
   b) $= |W|W_x$,
   c) Water level at Keszthely (1) and Kenese (2),
      respectively, together with observations,
   d) Discharge at Tihany (-.- from observations)
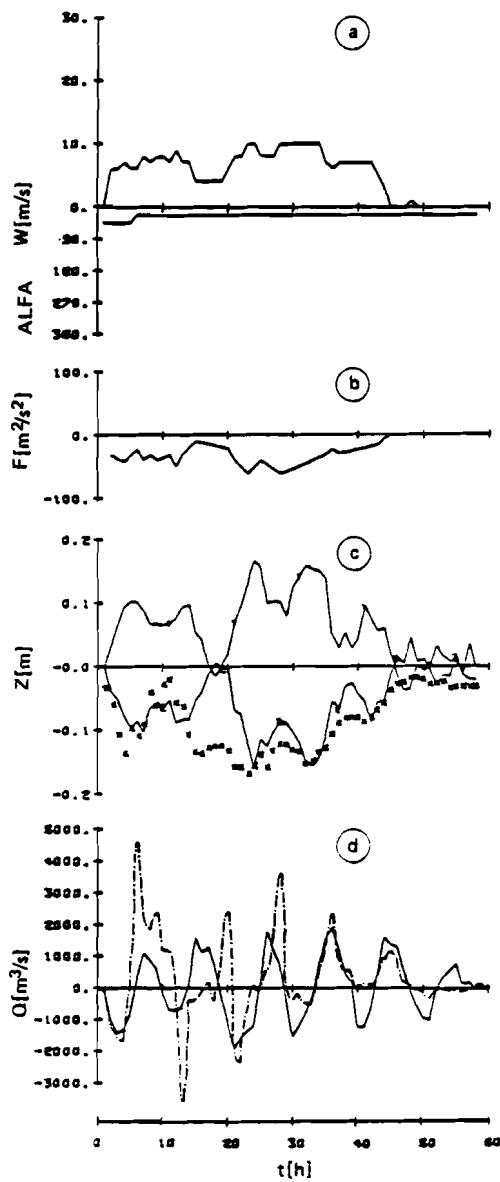
Figure 22. Simulation of a storm, 19.9.1965
 a. Wind speed and direction at Szemes,
 b. $F = |W|W_x$,
 c. Water level at the two ends of the lake
    (with observations at Keszthely,
 d. Discharge at Tihany (-.- from observations)
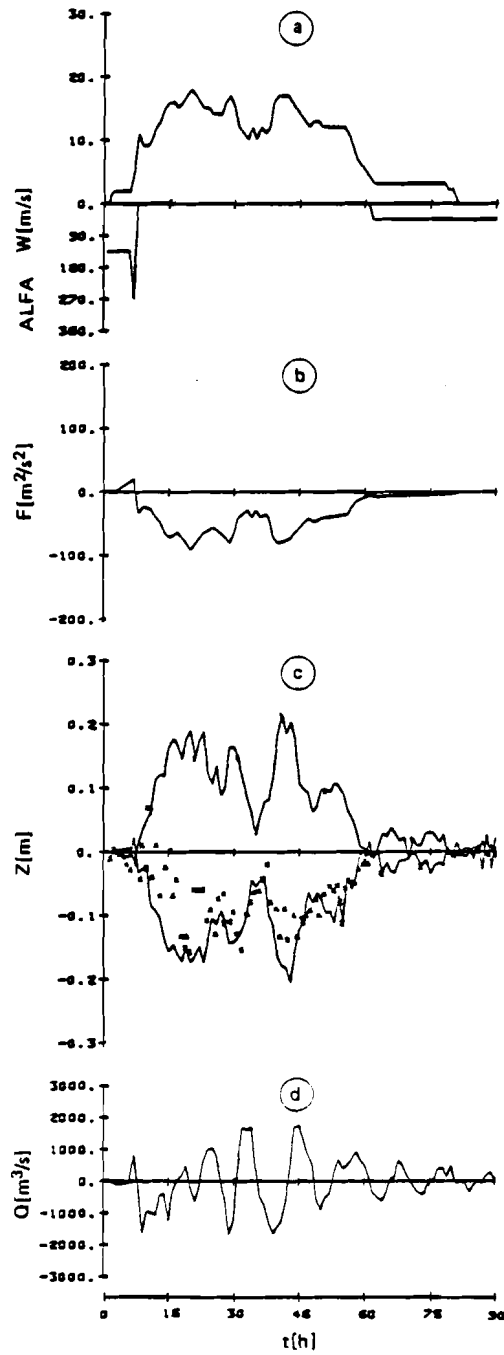
Figure 23. Simulation of a storm, 8.7.1967
 a. Wind record at Szemes,
 b. $F = |W|W_x$
 c. Water levels at Keszthely (with observations)
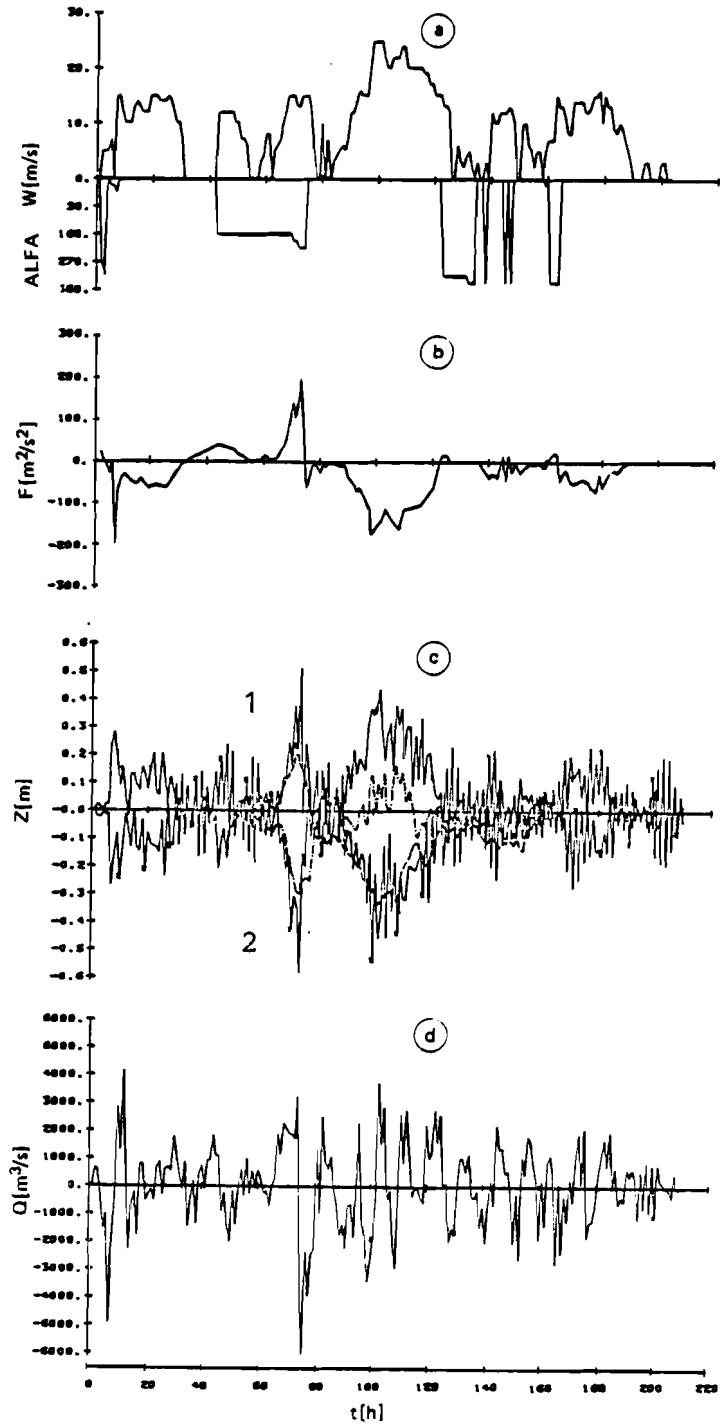   and Kenese
 d. Discharge at Tihany
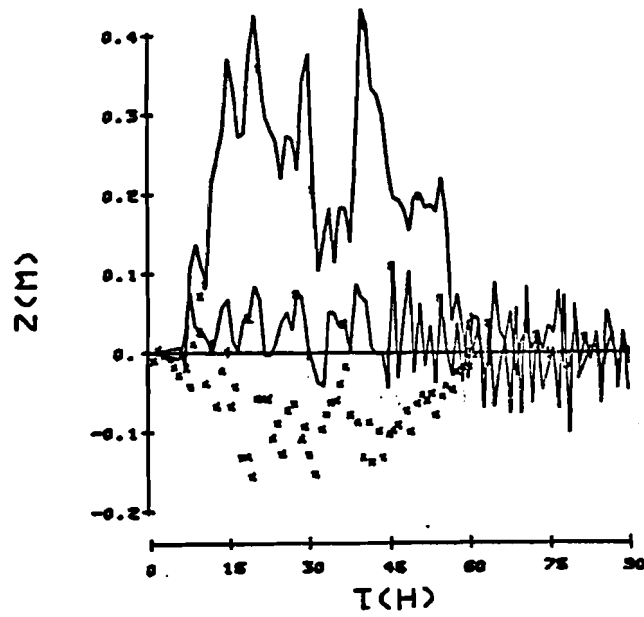
Figure 24. Sensitivity of the solution on spatial
changes in wind direction (storm of 8.7.1967)

-78-
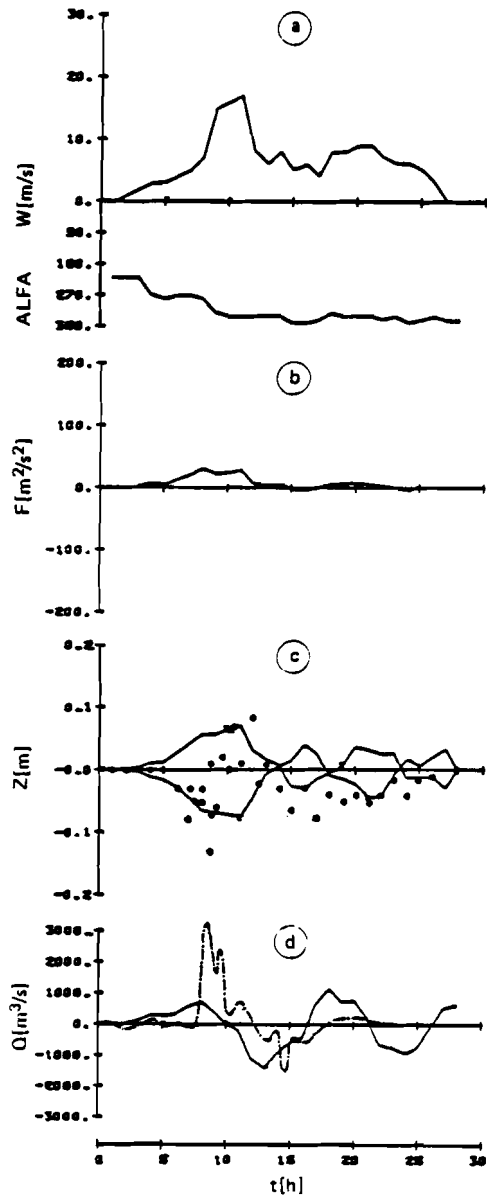
Figure 25. Simulation of a storm, 8.7.1963
          a. Wind record at Szemes, b. F = $|W|W_x$,
          c. Water levels at Keszthely (with observations)
             and Kenese,
          d. Discharge at Tihany (-.- from observations)

Figure 26. Simulation of a storm, 18.4.1967
       a. Wind record of Szemes, b. $F = |W|W_x$,
       c. Water levels at Keszthely (1) and
          Kenese (2),
       d. Discharge at Tihany
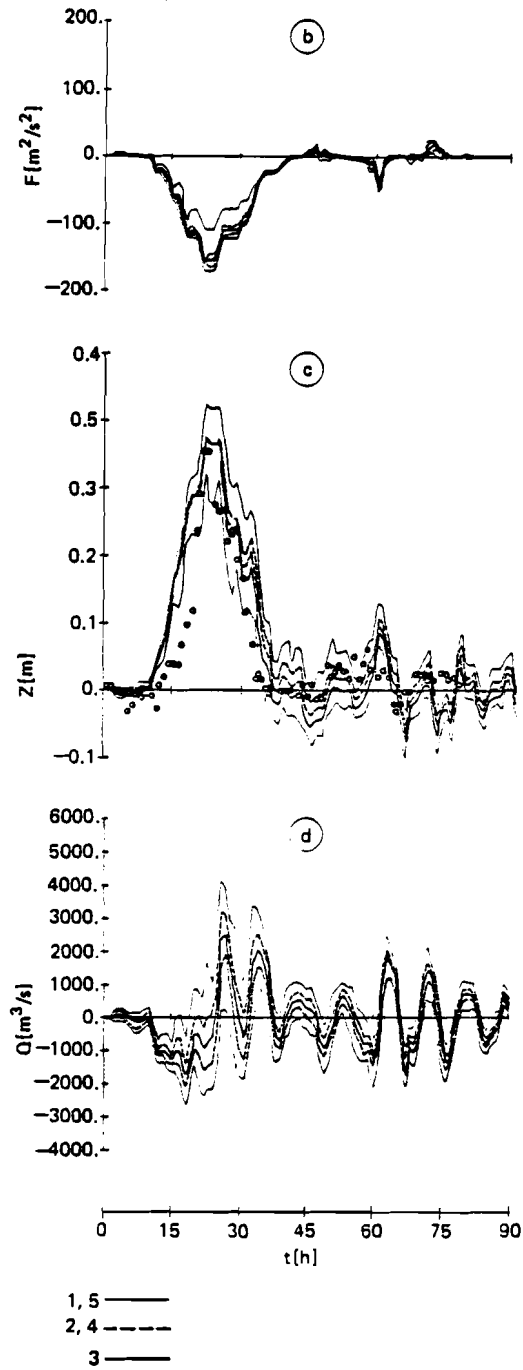
Figure 27. Results of Monte Carlo simulation for the storm
of 16.11.1966
b. $F = |W|W_x$, c. Water level at Keszthely together
with observations, d. Discharge at Tihany;
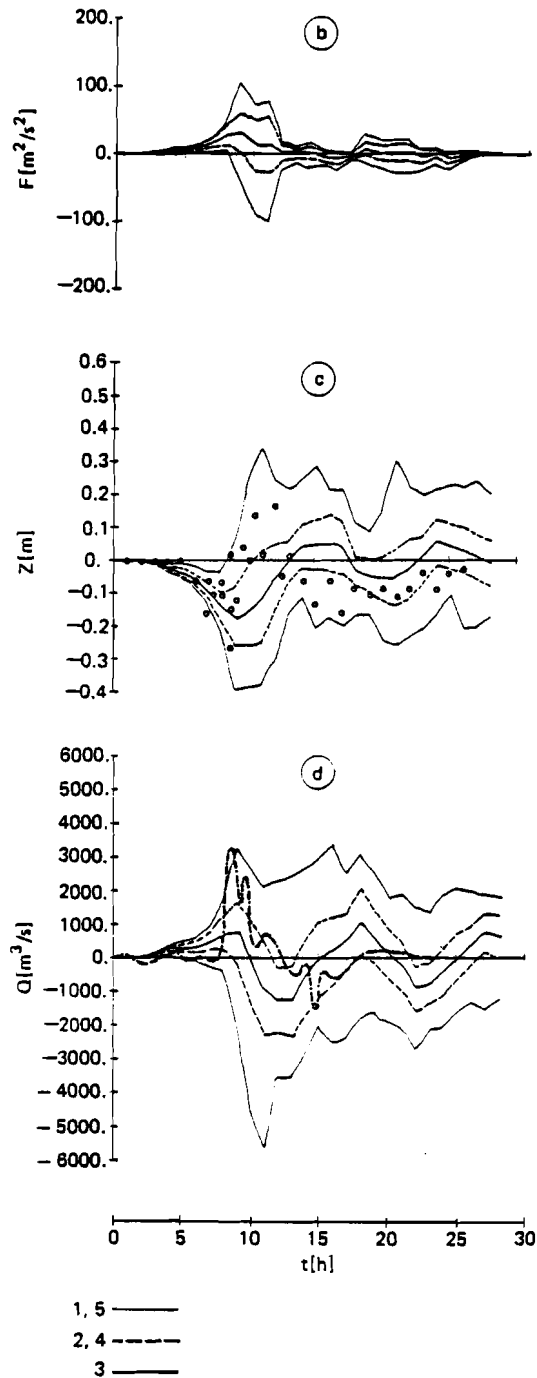3 - mean value, 4 and 2+ standard deviation,
1 and 5 extreme values

Figure 28. Monte Carlo simulation for the storm of 8.7.1963
b. $F = |W|W_x$. c. Water level at Keszthely with
observations, d. Discharge at Tihany; 3 - mean values,
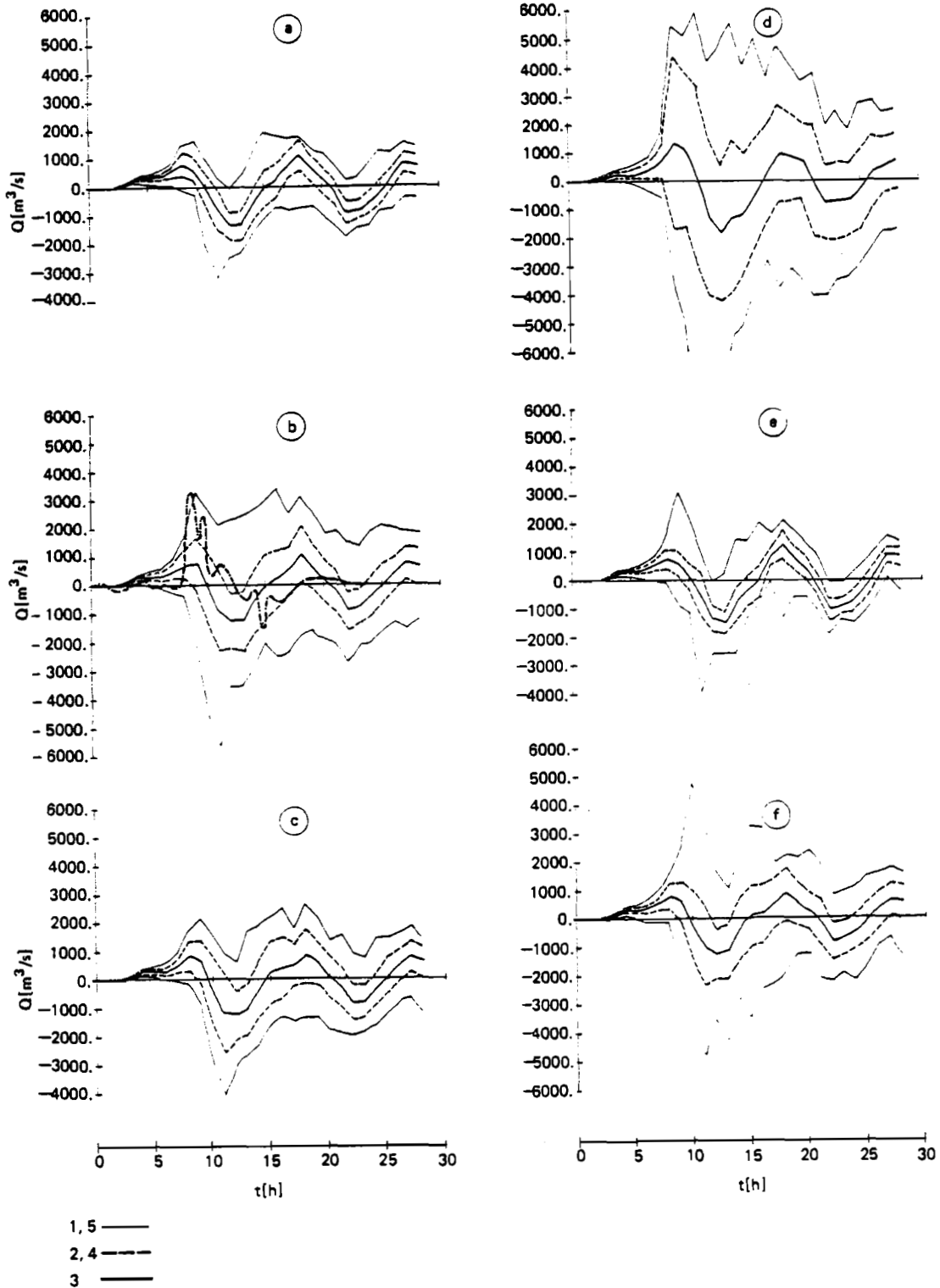2 and 4 ± standard deviations, 1 and 5 extreme values

-82-

Figure 29. Discharge at Tihany besides various types of wind
           uncertainties (3 mean, 2 and 4 ± standard deviation,
           1 and 5 extremes)
           a. Uniform distribution half range 22.5°,
           b. basic case with observations (uniform distribution
              33.8°), c. "discrete" distribution (half range
              22.5°), d. "discrete" distribution, 45°,
           e. Gaussian distribution, standard deviation, 11.3°,
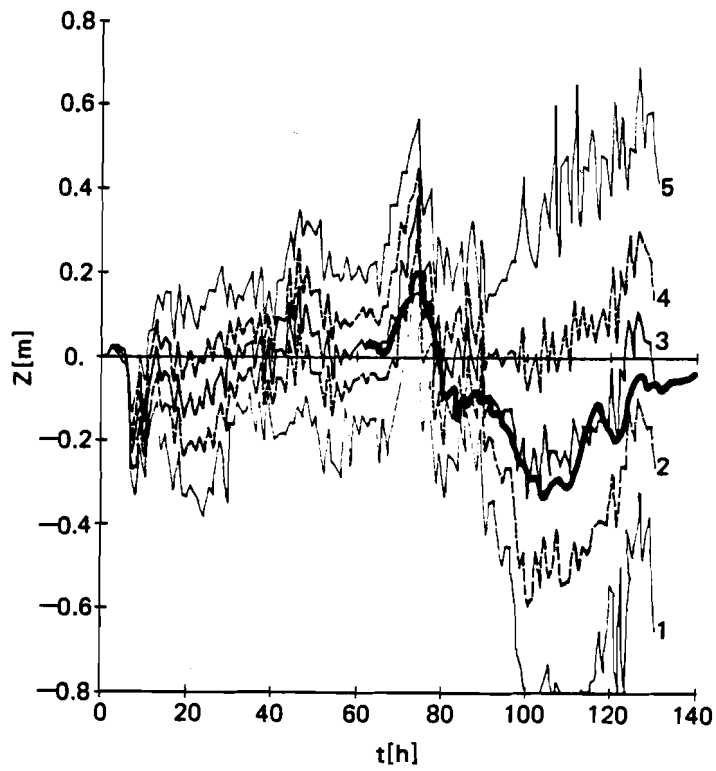   f. Gaussian distribution, standard deviation 16.8°.

Figure 30. Results of Monte Carlo simulations of the storm
of 18.4.1967 (e - mean, 2 and 4 ± standard deviation,
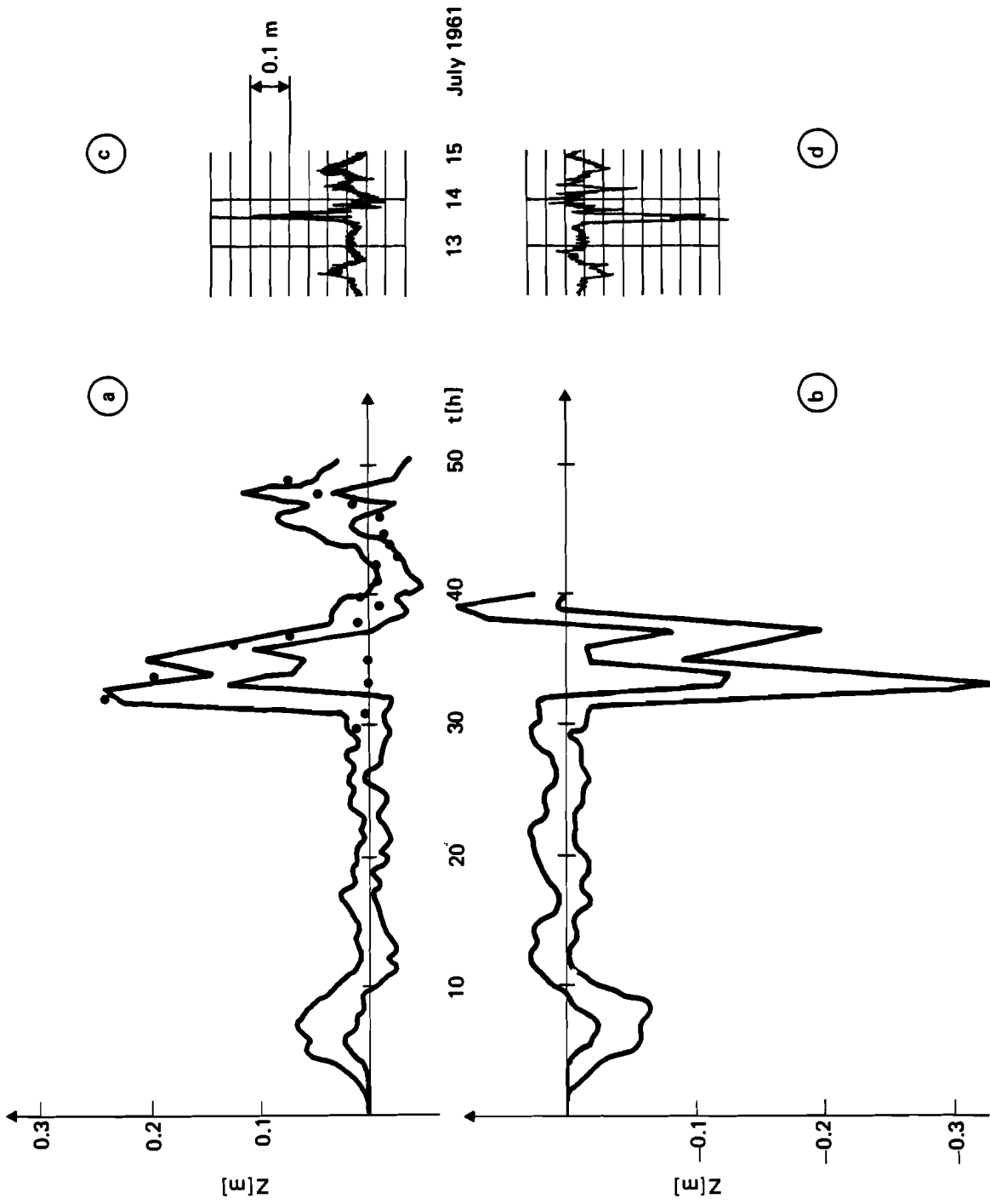1 and 5 extremes).

-84-

Figure 31. Envelopes of Monte Carlo simulations of the storm of 13.7.1961
a. Water level at Keszthely, b. Water level of Kenese,
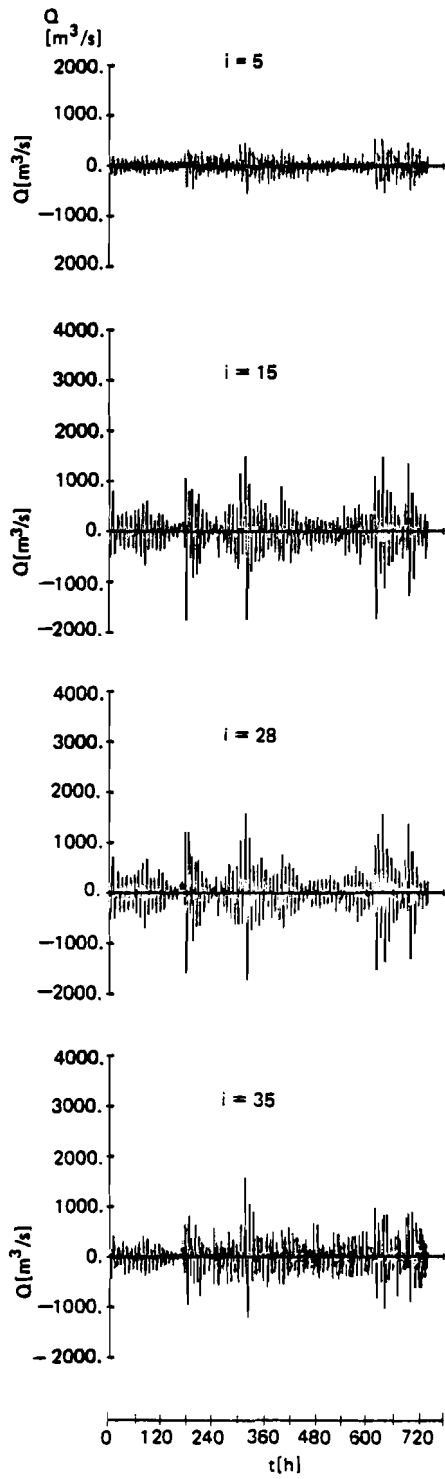c. and d. Continuous records (Muskalay, 1973)

Figure 32. Simulated streamflow for various locations of the lake, 1977 January
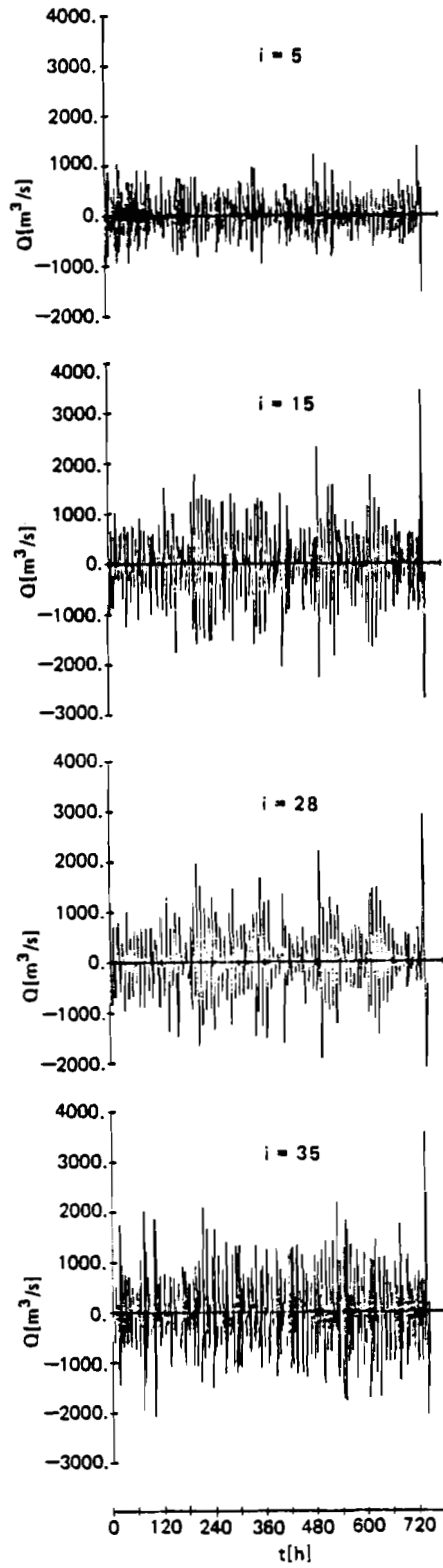
Figure 33. Simulated streamflow for various locations of the
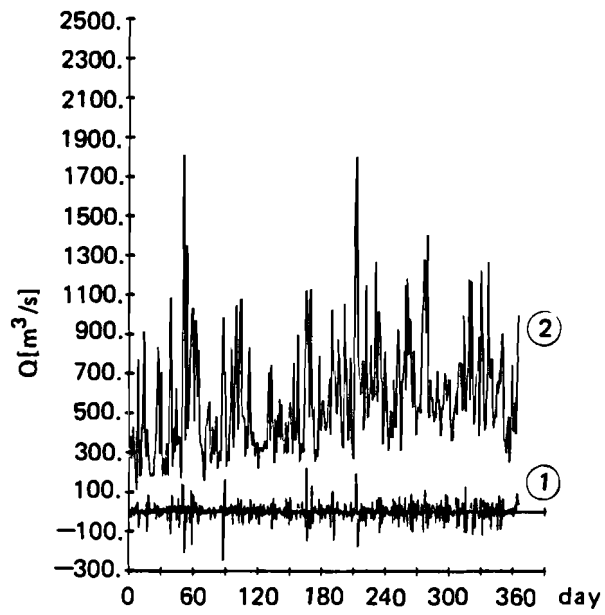lake, 1977 July

Figure 34. Daily mean and standard deviation of the
discharge at Tihany derived from hourly
values: simulation for 1977

REFERENCES

Béll, B. and L. Takács, eds. 1974. The climate of the Lake Balaton region. Hungarian Meteorological Institute, Vol. XL (in Hungarian).

Boyce, F.M., A.S. Fraser, E. Halfon, et al. 1979. Assessment of water quality simulation capability for Lake Ontario. Scientific Series No. 111. Inland Water Directorate, National Water Research Institute, Canada Centre for Inland Waters: Burlington, Ontario, p. 220.

Fischer, M.B., J. Imberger, E.J. List, et al. 1979. Mixing in inland and coastal waters. New York: Academic Press.

Graf, W.H., and J.P. Prost. 1980. Aerodynamic drag and its relation to the sea state: with data from Lake Geneva. Arch. Met. Geoph. Biokl., Ser. A, 29: pp. 67-87.

DP. Györke, O. 1975. Studies on the factors affecting the morphological processes in shallow lakes by means of a hydraulic model. 16th Congress, IAHR, Sao Paulo, Brazil, Paper B4, Vol. 2, p. 24.

Harleman, D.R.F., and P. Shanahan. 1980. Aspects of wind-driven circulation and mixing in eutrophication studies of Lake Balaton. Pages 50-67, Vol. 1. Proceedings of the Second Joint MTA/IIASA Task Force Meeting on Lake Balaton Modeling. G. van Straten, S. Herodek, J. Fischer, and I. Kovacs, eds. Veszprém, Hungary: MTA VEAB.

Jolánkai, G., and L. Somlyódy. 1981. Nutrient loading estimate for Lake Balaton. Collaborative Paper 81-21. Laxenburg, Austria.

International Institute for Applied Systems Analysis.

Kozák, M. 1977. Numerical modeling of lake currents. Annual Review of Earth and Planetary Sciences 4: 49-74.

Mahmood, K., and V. Yevjevich, eds. 1975. Unsteady flow in open channels. Fort Collins: Water Res. Publications, Vol. 1.

Muszkalay, L. 1973. Characteristic water motion in Lake Balaton. Budapest, Hungary. VITUKI (in Hungarian).

Muszkalay, L. 1979. Water motion in Lake Balaton. Summary of research results for Lake Balaton. Pages 34-128. S. Baranyi, ed. Budapest, Hungary. VIZDOK (in Hungarian).

Shanahan, P., D.R.F. Harleman, and L. Somlyódy. 1981. Modeling wind-driven circulation in Lake Balaton. Collaborative Paper 81-7. Laxenburg, Austria. International Institute for Applied Systems Analysis.

Shanahan, P. 1981. Linked hydrodynamic and biochemical models of water quality in shallow lakes. Ph.D. dissertation, Massachusetts Institute of Technology, Cambridge, Massachusetts.

Somlyódy, L. 1979. Hydrodynamical aspects of eutrophication modeling in the case of Lake Balaton. Collaborative Paper 79-1. Laxenburg, Austria. International Institute for Applied Systems Analysis.

Somlyódy, L. 1980. Preliminary study on wind-induced interaction between water and sediment for Lake Balaton (Szemes Basin). Proceedings of the Second Joint MTA/IIASA Task Force Meeting on Lake Modeling, G. van Straten, S. Herodek, J. Fischer, I. Kovács, eds. Veszprém, Hungary. MTA VEAB.

van Straten, G., G. Jolánkai, and S. Herodek. 1979. Review and evaluation of research on the eutrophication of Lake Balaton--a background report for modeling. Working Paper 79-13. Laxenburg, Austria. International Institute for Applied Systems Analysis.

van Straten, G., and L. Somlyódy. 1980. Lake Balaton eutrophication study: present status and future program. Working Paper 80-87. Laxenburg, Austria. International Institute for Applied Systems Analysis.

Virtanen, M. 1978. Computation of two-dimensional unsteady flow in shallow water systems. Report prepared for the Ninth International Post-Graduate Course on Hydrological Methods for Developing Water Resources Management, UNESCO-VITUKI, Budapest, Hungary.

VITUKI. 1976. Standard cross-sections of Lake Balaton. Budapest, Hungary. VITUKI.

Wu, J. 1969. Wind stress and surface roughness at air-sea interface. Journal of Geophysical Research 74(2):444-455.